81p.

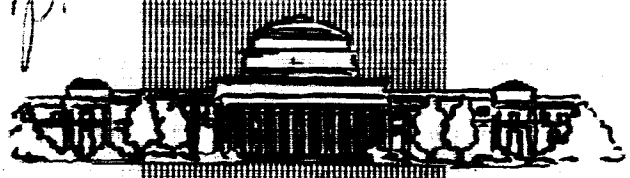

MASSACHUSETTS INSTITUTE OF TECHNOLOGY

A HIGH SENSITIVITY SOLID STATE LIGHT DETECTOR

by

Sanford Cohen

August 1963

Master of Science Thesis

TE-6

EXPERIMENTAL ASTRONOMY LABORATORY

MASSACHUSETTS INSTITUTE OF TECHNOLOGY

CAMBRIDGE 39, MASSACHUSETTS

TE-6

A HIGH SENSITIVITY SOLID STATE LIGHT DETECTOR

by

Sanford Cohen (M.S. Thesis) Aug. 1963 reg

B.E.E., City College of New York, 1959

Submitted in Partial Fulfillment
of the Requirements for the
Degree of Master of Science
at the

MASSACHUSETTS INSTITUTE OF TECHNOLOGY (Cambridge) 5545009

August 1963

Signature of Author Sanford Cohen
Department of Aeronautics and Astronautics, August, 1963

Certified by W. Markey
Thesis Supervisor

Accepted by W. Wrigley
Chairman, Departmental Graduate Committee

ACKNOWLEDGMENT

The author wishes to express his appreciation to Professor Winston R. Markey, who as thesis supervisor guided this investigation.

Special thanks are also due Mr. Joel B. Searcy, Mr. Philip K. Chapman, and Bernard E. Blood of the Experimental Astronomy Laboratory for their untiring guidance and criticism.

This research was carried out under DSR contract 9406, sponsored by NASA under purchase order number NsG254-62.

A HIGH SENSITIVITY SOLID STATE LIGHT DETECTOR

by

Sanford Cohen

Submitted to the Department of Aeronautics and Astronautics on 19 August 1963 in partial fulfillment of the requirements for the degree of Master of Science.

ABSTRACT

13068

A gallium arsenide photovoltaic cell is combined to a field effect transistor making a solid state light detector. This detector is found to be capable of sensing stellar radiation.

AUTHOR

Thesis Supervisor: Winston R. Markey

Title: Associate Professor of Aeronautics and Astronautics

TE-6

A HIGH SENSITIVITY SOLID STATE LIGHT DETECTOR

OBJECT

The object of this thesis is to investigate a high sensitivity solid state light detector suitable for low level light sensing, consisting of a gallium arsenide photovoltaic cell and a field effect transistor.

by Sanford Cohen

LIST OF SYMBOLS

GaAs	Gallium Arsenide
E	Electric Field
h	Planck's Constant
ν_o	Lowest Detectable Photon Frequency
c	Speed of Light
λ_o	Long Wavelength Cutoff
N_r	Response Noise or Diode Noise
b	An Applied Bias
r	Detector Response
Δf	Bandwidth
NEP	Noise Equivalent Power
I_L	Cell Current
R_D	Cell Resistance
C_D	Cell Capacitance
N_λ	Fraction of the Photon Generated Hole-Electron Pairs
ϵ_λ	Quantum Efficiency of the Excitation Process
A	Surface Area
I_λ	Monochromatic Photon Flux Density
J_s	Saturation Current Density of the Junction
q	Electron Charge
F.E.T.	Field Effect Transistor
R_o	Resistance of the F.E.T. Channel
ρ	Resistivity of the Channel
L	Length of Channel

LIST OF SYMBOLS (Continued)

z	Width of Channel
a	Half Height of Channel
σ	Conductivity of Channel
W_o	"Pinch-Off" Voltage
ρ_o	Charge Density
N	Electron Density
V_g	Gate Voltage
I_c	Collector Current
β	DC Current Gain
I_b	Base Current
g_m	Transconductance of F.E.T.
V_{gc}	Gate to Cathode Voltage
R_L	Load Resistance
V_o	Output Voltage
A_v	Voltage Gain of the Detector
R_s	Shunt Resistance
Z_c	Capcitive Impedance
f	Frequency
S/N	Signal to Noise Ratio
N.D.	Neutral Density
P	Radiant Power
I	Anode Current
S_K	Radiant Sensitivity of IP21

LIST OF SYMBOLS (Continued)

P_{LLD}	Lower Limit Radiant Power of Detector
S_{DR}	Radiant Sensitivity of Detector
P_{LLM}	Lower Limit Radiant Power of IP21
S_{DL}	Luminous Sensitivity of Detector
F	Fabre Number
A_{ol}	Area of the Objective Lens
L_p	Luminous Power
e_s	Signal Voltage at the Output of the Detector
e_{nrms}	Equivalent rms Noise Voltage at the Input to the Detector
m_v	Visual Magnitude

TABLE OF CONTENTS

TABLES

LIST OF ILLUSTRATIONS

CHAPTER I
INTRODUCTION

The classical photovoltaic cell utilizes an effect discovered in 1865 by Becquerel.[1] In this first cell and for many that followed, electrodes made of copper plates coated with cuprous oxide were immersed in a solution of copper salt. When one of these electrodes was illuminated, a potential difference was generated which was approximately proportional to the intensity of the illumination. Photovoltaic cells have come a long way since their discovery nearly a century ago. Today solid state detectors, as opposed to the first electro-chemical detectors, are in common usage—from supplying electrical energy for our artificial earth satelites, to turning on our cities' street lamps at dusk.

Many of these more commonly known detectors such as selenium, do not have very high sensitivities and for the past thirty years the multiplier phototubes despite their size, high voltage requirement, and inherent microphonics, have had to be used where low light intensities, such as from stellar radiation, had to be measured. Today there are semiconductor cells available which can measure visible light at very low levels, among these are silicon photoconducting diodes and gallium arsenide photovoltaic cells.

Common to all of these detectors is their high output impedance necessitating complicated and very special purpose electronics in order to make them useful for low light level detection.[2]

If these cells could be matched to rather simple high input impedance amplifiers, much the same as the photoemissive

surface was matched to the electron multiplier to give the photomultiplier tube, then their usefulness would be greatly enhanced. Such a match is the basis of this investigation. The field-effect transistor, which like the vacuum tube pentode is a very high input impedance, voltage controlled device, is combined to the GaAs photovoltaic cell. This combination does not exhibit the microphonics associated with photomultiplier tubes nor the inconvenience and expense of high voltage power supplies, it also affords an appreciable saving in volume and weight over the photomultiplier tube.

CHAPTER II
THE GALLIUM ARSENIDE PHOTOVOLTAIC CELL

2.1 General

Solid State photon detectors can be placed into two categories: intrinsic and impurity activated detectors. Intrinsic detectors consist of compounds containing two basic elements in stoichiometric proportions, such detectors are PbS, PbSe, PbTe, InSb, and InAs to name but a few.[3, 4] Photoconductivity in these detectors is produced when impinging photons liberate charge carriers from atoms of the compound. When photons hit the surface of an impurity activated semiconductor device free hole electron pairs are produced.[5, 6]

The requirement imposed upon the photon energy for either type is that it be sufficient to cause excitation. If $\Delta\mathcal{E}$ is the minimum energy required, representing the width of the forbidden band, then we have,

$$\Delta\mathcal{E} = h\nu_o = h\frac{c}{\lambda_o} \qquad (2\text{-}1)$$

where ν_o is the lowest detectable photon frequency, λ_o is the longest detectable wavelength, and c is the speed of light. Frequencies greater or wavelengths shorter than these will still produce excitation, the excess energy lifting the carriers into higher lying free states corresponding to kinetic energy imparted to the carrier. For $\Delta\mathcal{E}$ expressed in electron volts and λ_o in microns, the long wavelength threshold is

$$\lambda_o = \frac{1.24}{\Delta\mathcal{E}} \qquad (2\text{-}2)$$

The photovoltaic effect in a general p-n junction is discussed in the next section and the succeeding sections deal with the characteristics of the gallium arsenide photovoltaic p-n junction.

2. 2 Photovoltaic Effect in a p-n Junction

To explain the photovoltaic effect fully one must go back to the basic energy level diagram of a p-n junction which is reproduced as Fig. 2. 1.[5, 6, 7, 8]

In the absence of radiation falling upon the junction, the Fermi levels in the p and n regions are aligned. An internal electric field E, the direction of which is shown by the arrow, exists at the potential barrier (junction). This electric field exists due to the initial diffusion of holes across the junction into the n-type region and electrons into the p-type region. This potential constitutes a potential energy barrier against the further diffusion of holes across the barrier. Therefore, when a photon of wavelength sufficiently short to cause excitation is absorbed at the barrier and a hole-electron pair is produced, it is the action of the electric field at the barrier which separates the pair, moving the electron into the n-type material and the hole into the p-type material. Since excess electrons have moved into the n-type region, and excess holes into the p-type region, the n-type region becomes charged negatively and the p-type positively. As long as radiation falls upon the junction, electron-hole pairs will be formed and separated by the internal field at the junction. If the semiconductor ends are short circuited by an external conductor, a current will flow in the circuit as long as radiation falls upon the junction. On the other hand, if the semiconductor ends are terminated in a very high impedance, then a voltage can be measured across the impedance that is proportional to the incident radiation upon the junction.

So far only that radiation absorbed at the barrier has been discussed. The radiation that falls on the n and p type region sufficiently remote from the barrier will cause no photovoltaic effect. If, however, excess carriers are generated close enough to the barrier so as to diffuse there and be separated, then a photovoltaic effect will be observed. The magnitude of

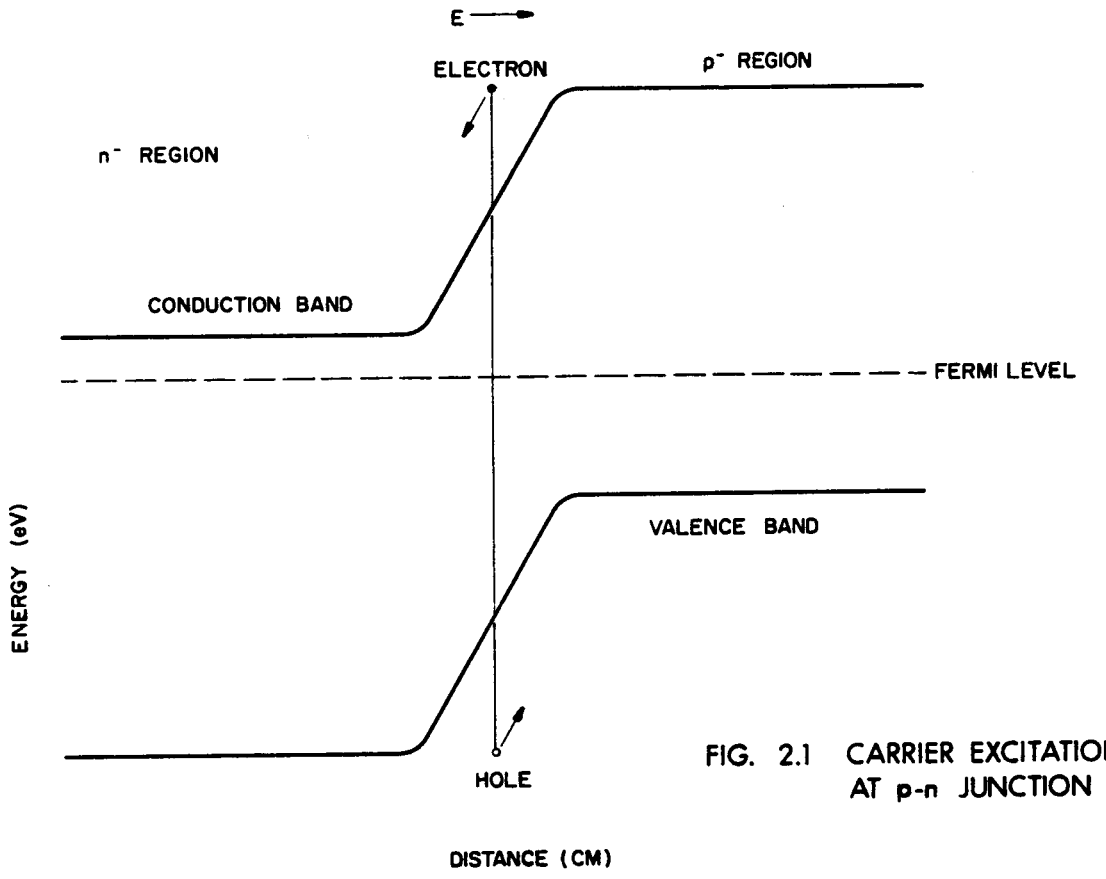

FIG. 2.1 CARRIER EXCITATION AT p-n JUNCTION

the photovoltaic effect for a constant intensity of the exciting radiation is a function of the distance from the point of excitation to the barrier. Those carriers which are excited one diffusion length away from the barrier and diffuse toward the barrier, will suffer recombination along the way so that only $\frac{1}{e}$ of the original number arrive at the barrier and contribute to the photovoltage. Those excited closer to the barrier will arrive in greater numbers.

It is possible to reverse bias the photovoltaic p-n junction and use the device as a photodiode.[8, 9] However, this use usually limits the sensitivity because of the added diode noise component.[3] In order to get the greatest sensititvty from the photovoltaic cell it should be used in conjunction with a very high input impedance low noise amplifier.

2.3 The Gallium Arsenide Photovoltaic p-n Junction

The gallium arsenide detector is shown in Fig. 2.2.[10] The area of the cell used in the experimentation was 1 mm^2 and was purchased from the Philco Corp., Lansdale, Pennsylvania. The commercial type number is GAU-401.

The p-n junction is formed in n-type GaAs by a diffusion technique. The depth of the junction below the surface is much less than a minority carrier diffusion length and thus an appreciable fraction of the generated pairs reach the junction, and as outlined in the preceding section thereby contribute to the photovoltage. It is the current state of the art of transistor manufacturing that has allowed such narrow diffusion depths. Prior to the attainment of such narrow depths all such devices had to be used in the photodiode mode of operation[9] because the hole-electron pairs that were generated recombined along the way and resulted in only $\frac{1}{e^3}$ (for three minority carrier diffusion lengths between surface and barrier), or less, of the original photon generated hole-electron pairs to contribute to the photovoltage. By being able to keep the diffusion depths very narrow the inherent sensitivity of the device operating in the photovoltaic mode can be made greater than when it is operating in the photoconducting mode due to the absence of response noise (N_r) or diode noise. This noise is given by[3] (See Appendix B)

$$N_r^2 \propto b^x r^2 \Delta f \qquad (2\text{-}3)$$

where b is an applied bias and necessary for photodiode operation, x is a constant generally equal to one, and r is the detector response. For zero applied bias, that is operating in the photovoltaic mode, it is seen that this noise contribution is zero.

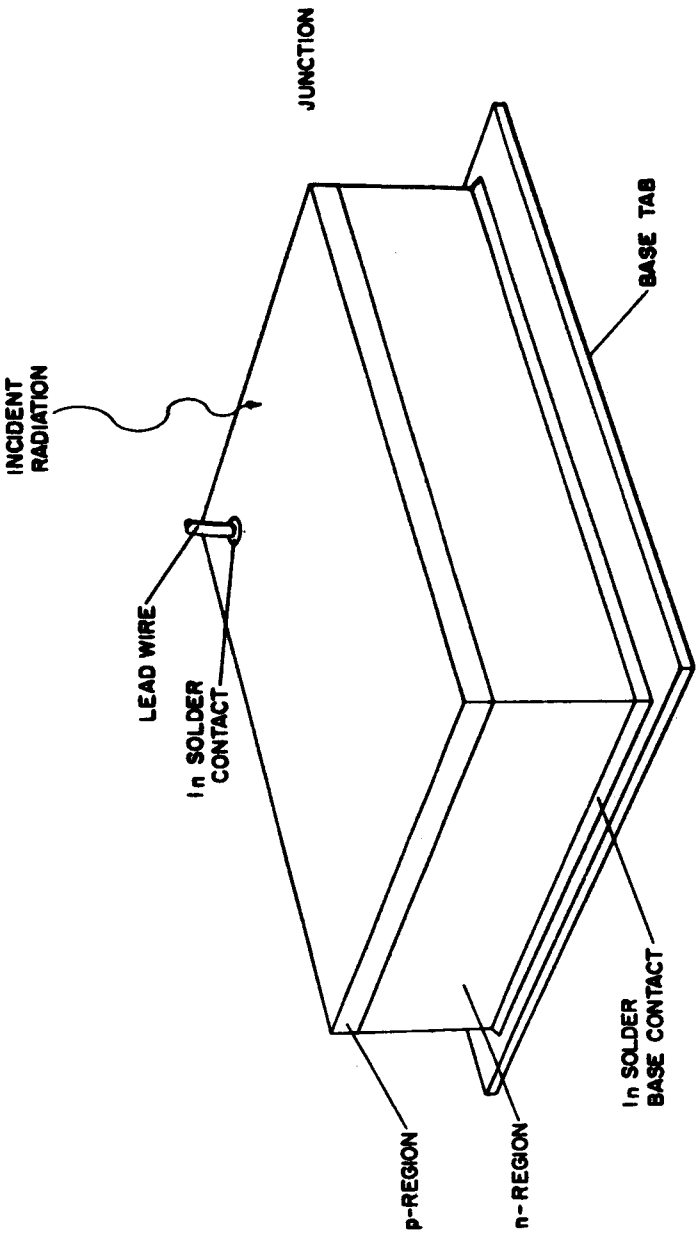

FIG. 2.2 PHYSICAL CONSTRUCTION OF THE GaAs PHOTOVOLTAIC DECTECTOR

Nonrectifying Indium contacts are found on both the n and p regions and the donor density[6] is about $3.7 \times 10^{17}/cm^3$ at 300° K.

Figure 2.3 contains the monochromatic sensitivity curve of the gallium arsenide cell, (Philco GAU-401). The cell has a peak sensitivity at 0.85μ. The half sensitivity points are at 0.91μ and 0.56μ. For a definition of NEP see Appendix A.

The manufacturer's electrical characteristics are outlined in Table 2.1.

TABLE 2.1

Electrical Characteristics of the GaAs Cell

Cell Impedance	1.5 megohms
Cell Capacitance	350 pf
Area	1 mm^2
Position of Spectral Peak	0.85 microns
NEP (See Appendix A) At Special Peak	5×10^{-13} watts

Figure 2.4 contains a plot of photovoltage vs. incident effective flux density (See Appendix A) and indicates that the cell is linear in the low flux density region.

The equivalent circuit of the cell is given in Fig. 2.5a and the equation describing its response is

$$V(\omega) = \frac{I_L R_D}{\left[1 + (R_D C_D)^2 \omega^2\right]^{1/2}}$$

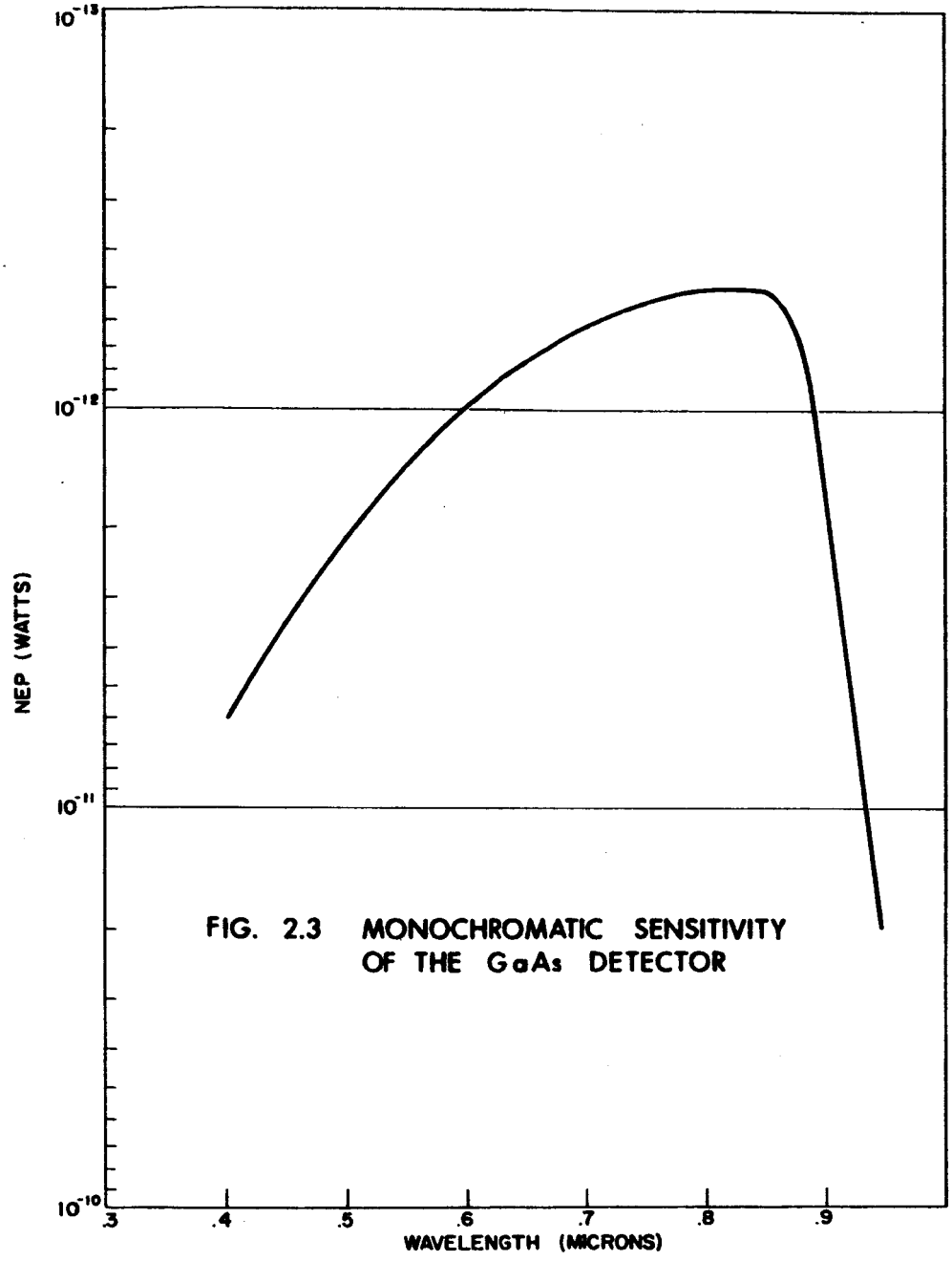

FIG. 2.3 MONOCHROMATIC SENSITIVITY OF THE GaAs DETECTOR

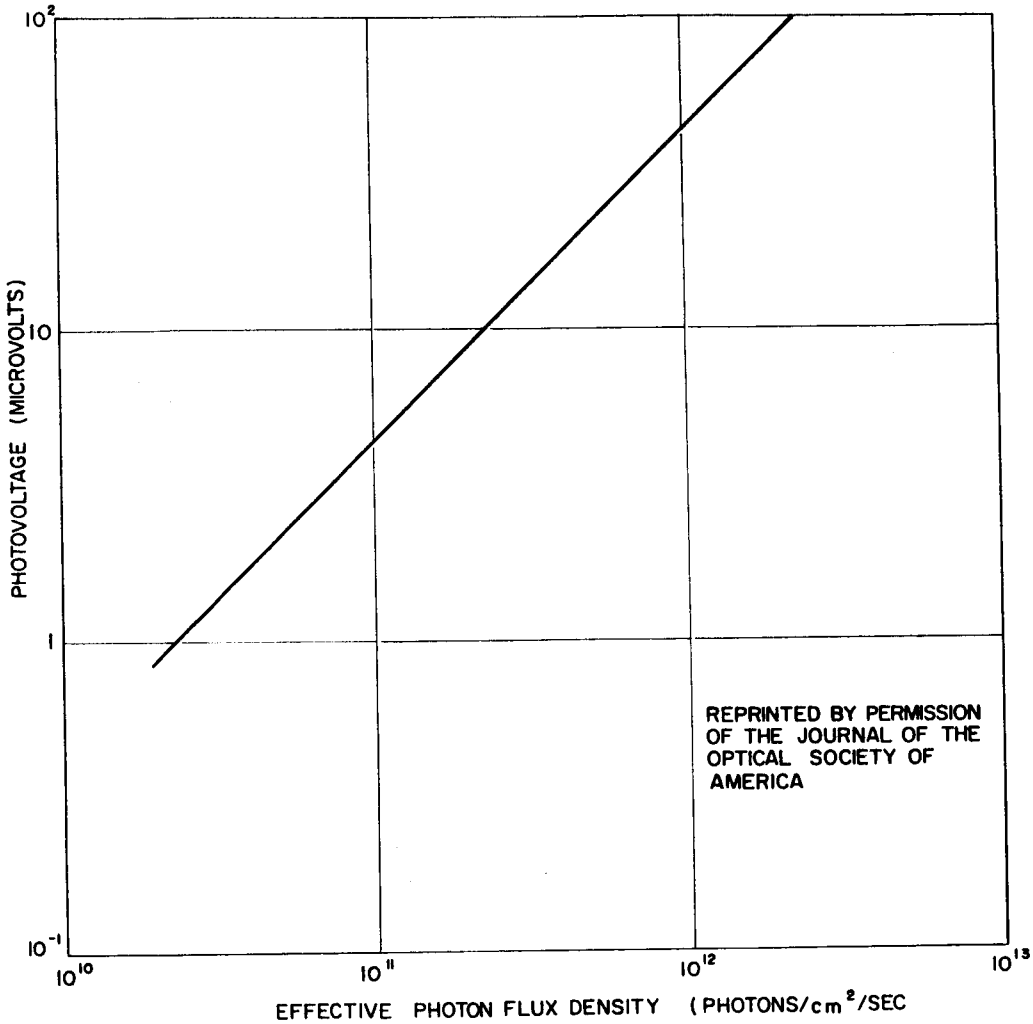

FIG. 2.4 PHOTOVOLTAGE VS. INCIDENT EFFECTIVE FLUX DENSITY FOR THE GaAs DETECTOR

where[10]

$$I_L = A\int_o^{\lambda_o} \eta_\lambda \epsilon_\lambda I_\lambda d\lambda \qquad (2\text{-}4)$$

where η_λ is the fraction of the photon generated hole-electron pairs that contribute to the photovoltage, ϵ_λ is the quantum efficiency of the excitation process, A the surface area, and I_λ is the monochromatic photon flux density in the interval from λ to $\lambda + d\lambda$; also, λ_o is the long-wavelength cutoff of the cell. For the small signal case R_D is a constant and is given by[10]

$$R_D = \frac{KT}{A_q J_s} \qquad (2\text{-}5)$$

where J_s is the saturation current density of the junction. The barrier capacitance of the detector C_D is constant.

The noise equivalent circuit is given in Fig. 2. 5b and consists of junction shot noise which is very small for the photovoltaic mode, Johnson noise of the junction resistance and "one over f" $(\frac{1}{f})$ noise which is generally attributed to surface effects and faulty contacts.

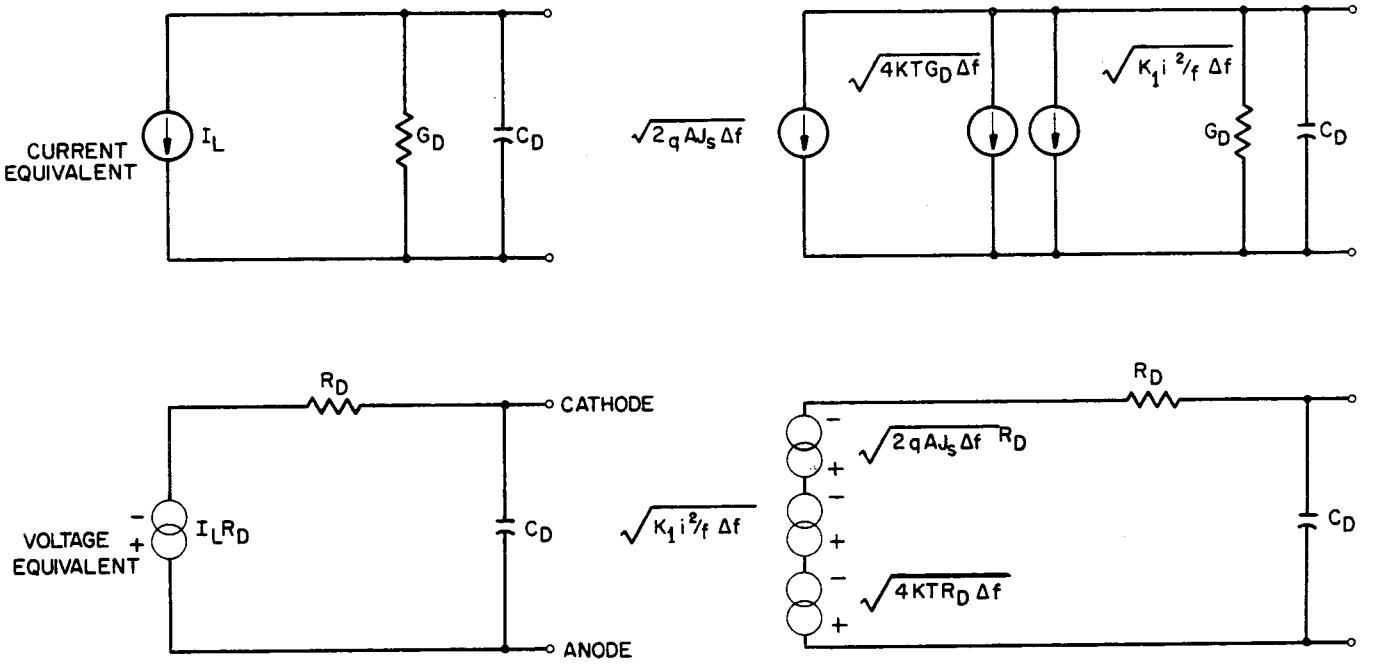

FIG. 2.5a SMALL SIGNAL EQUIVALENT CIRCUIT OF GaAs DETECTOR

FIG. 2.5b NOISE EQUIVALENT CIRCUIT OF GaAs DETECTOR

CHAPTER III
THE FIELD EFFECT TRANSISTOR

3.1 General

The Unipolar Field Effect Transistor[6, 11] has low inherent noise characteristics, moderate gain and high input impedance, making it attractive for use as a preamplifier stage following a high output impedance transducer. The name Unipolar is derived from the fact that the device uses charge carriers of one polarity only, contrary to ordinary transistors which use both electrons and equivalent positive charges or holes.

3.2 Theoretical Background

The familiar transistor relies on the transit effect of charge carriers, but this is not the only effect which can be used in semiconductors. It is sufficient to recall, for example, the Hall Effect which creates a voltage between opposite faces of a semiconductor immersed in a magnetic field, or Peltier Effect, used in purely electronic refrigeration systems. Another phenomenon is field effect, which appears when a semiconductor junction is reverse biased.

In essence, a field effect transistor (F. E. T.) can be regarded as a structure containing a semiconducting current path, the conductivity of which is modulated by the application of a transverse electric field.

Figure 3.1 shows a slab of n-type Silicon. At either end there are two contacts made, the source and the drain respectively. The slab also carries two indium junctions on opposite sides. These p-n junctions constitute the gates. Under the voltage conditions specified in Fig. 3.1, current flows from drain to source. This current consists of electrons flowing through the n-type channel from source to drain. For small applied voltages the resistance, R_o of this channel is

$$R_o = \frac{\rho L}{A} = \frac{L}{2azc}$$

where

$$\rho = \frac{1}{\sigma}$$

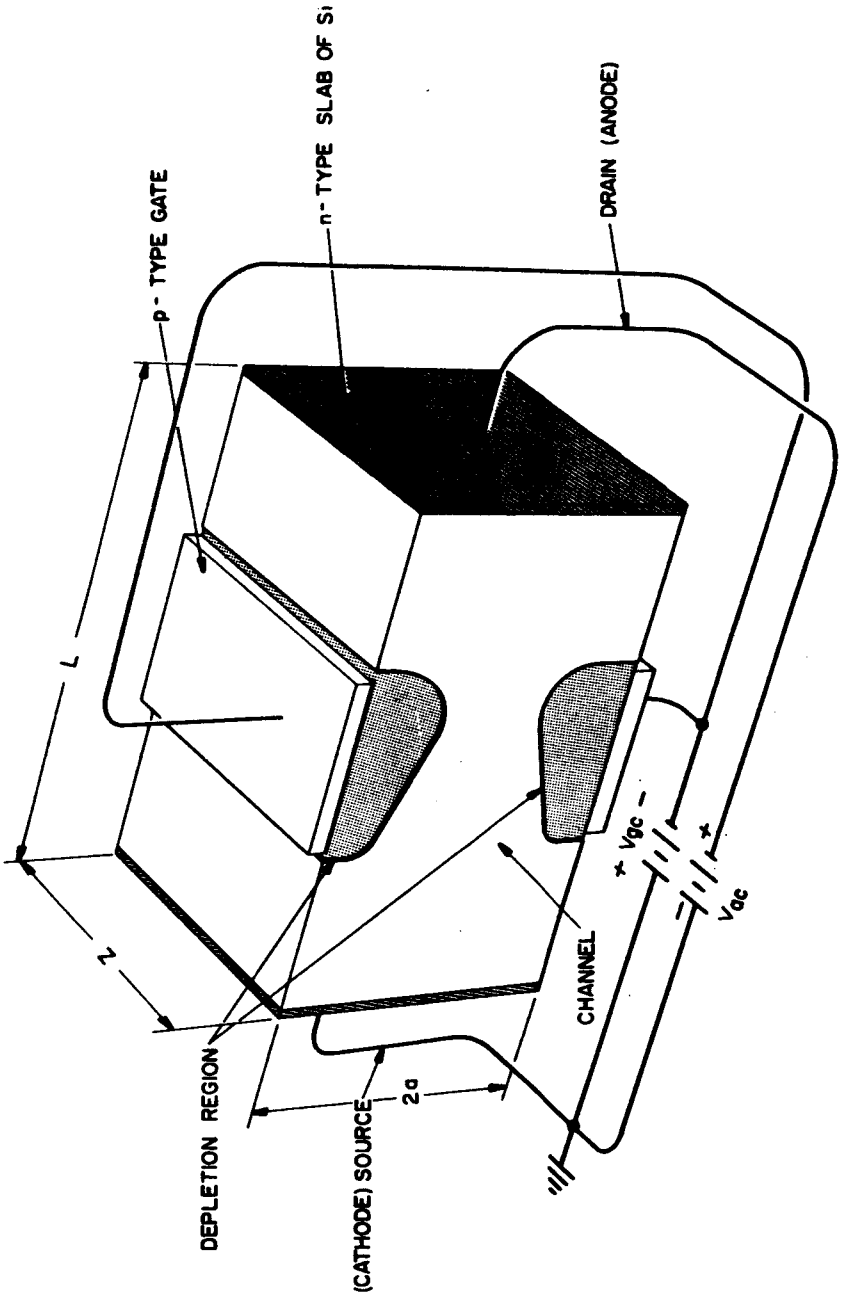

FIG. 3.1 PHYSICAL CONSTRUCTION OF THE FIELD EFFECT TRANSISTOR

and L, 2a and z are specified in Fig. 3. 1.

As the drain voltage is raised, more current flows in the channel, and the IR drop along the channel makes it more positive the greater the distance from the source. This means that those portions of the gate p-n junction which are most distant from the source will be biased more strongly in the reverse direction and a wedge shaped space-charge barrier will result. The space-charge region is shown dotted in Fig. 3. 1. The current flow is confined to the neutral channel. When the drain voltage reaches a critical value, W_o, the channel is completely "pinched-off"[12, 13] at its drain end. Virtually, no further increases of drain current will result when the drain voltage is raised above W_o, the only effect of this voltage being to change the channel shape at constant current. The value of this "pinch-off" voltage is[13]

$$W_o = \rho_o \frac{a^2}{2K}$$

where

$$\rho_o = \frac{1}{qN}$$

and

$$K = \text{dielectric constant}$$

If the gate is biased negatively with respect to source, then the magnitude of the IR drop necessary to produce "pinch-off" will be smaller, since part of this voltage is already supplied by the bias, Saturation will accordingly occur at a lower value of drain voltage and current.

If efficient resistance modulation is to be obtained, the semiconductor must be very thin between gates. A few tens of microns is a common value. This necessitates extreme care in the manufacturing process. Also, the working frequency

3.3 The Crystalonics Field Effect Transistor

The particular field effect transistor that was chosen for the purpose of this experiment was the Crystalonics C622.[14] The choice was made solely on the equivalent input noise of the device as stated in the manufacturer's specification sheet.

The output characteristic of the device is shown in Fig. 3.2. The electrical characteristics of the C622 are outlined in Table 3.1 and the equivalent circuit of the F. E. T. is given in Fig. 3.3 together with the nominal equivalent component values.

TABLE 3.1

Electrical Characteristics of the Crystalonics C622 Field Effect Transistor

Maximum Anode Current	50 ma
Maximum Dissipation	250 mw
Transconductance	75 micromhos
Grid Leakage Current	$< 10^{-9}$ amperes
Input Impedance	> 100 megohms
Input Capacitance	70 pf
Input Noise	$< 0.1\mu$ volts

In conclusion then, field effect is used to control the resistance of a slab of semiconductor material. A depletion layer appears in the semiconductor underlying the gates. The only conducting part is between the opposing gate space-charge regions, and is called the channel. The effect of the space-charge is to reduce the cross-section of the conducting zone; hence to increase the resistance of the Si slab, which in turn reduces the current

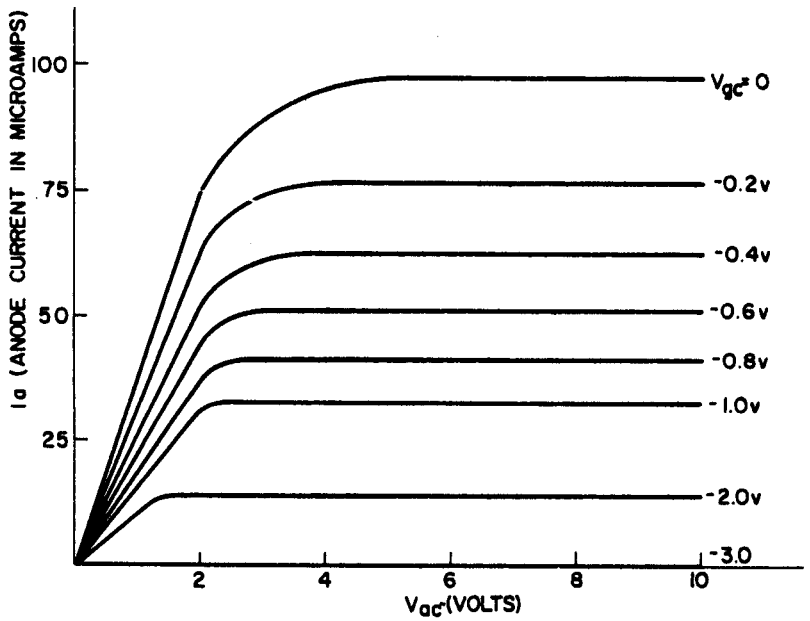

FIG. 3.2 OUTPUT CHARACTERISTIC OF THE CRYSTALONICS C622 FIELD EFFECT TRANSISTOR

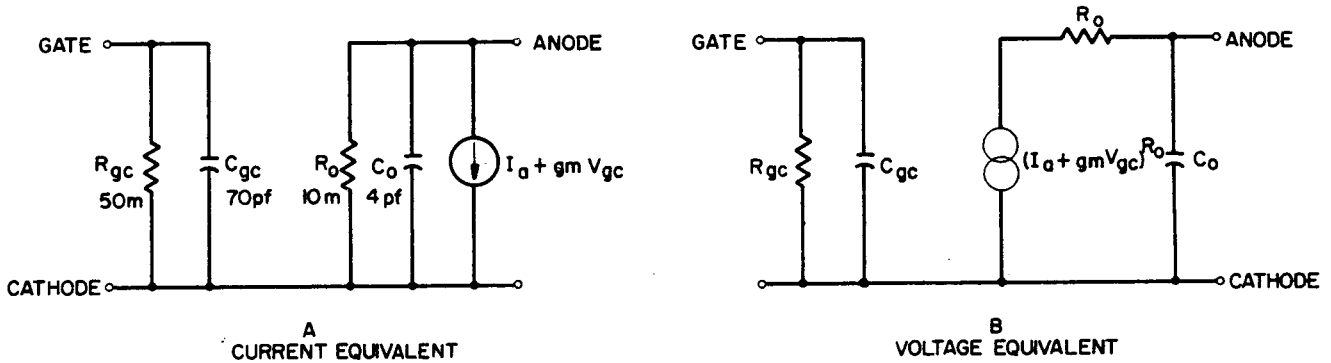

FIG. 3.3 SMALL SIGNAL EQUIVALENT CIRCUIT OF C622 FIELD EFFECT TRANSISTOR

due to drain voltage. This current can be controlled by modifying V_g, the gate voltage. Since V_g provides almost no current through the reverse biased junction, the device gives power gain and behaves as an amplifier.

CHAPTER IV
THE GaAs F. E. T. DETECTOR

This chapter deals with the characteristics of the experimental detector.* The technique used for finding the equivalent input noise can be found in Appendix C, while the experimental circuitry for the frequency response measurements is in Appendix D.

The basic design criterion for the preamplifier was simplicity, but at the same time it was to give operational improvement over existing high input impedance amplifiers. Complicated electronic circuits could be designed to meet given specifications, just as is done with photomultiplier tubes. However, this was not the objective of this thesis. Rather, it was to develop a general purpose laboratory tool that would hopefully be as sensitive and as simple to operate as a photomultiplier tube.

*Detector will mean GaAs surface followed by a field-effect transistor preamplifier.

4.1 The Field Effect Preamplifier

The preamplifier schematic is shown in Fig. 4.1 together with the equivalent circuit of the GaAs cell. The small signal current flowing out of the field-effect transistor is given by $g_m V_{gc}$ (refer to Fig. 3.3a)· this current flows directly into the base of a conventional transistor. The collector current of the 2N1613 is given by:

$$I_c = \beta I_b = \beta g_m V_{gc} \tag{4-1}$$

the output voltage is:

$$V_o = I_c R_L = \beta g_m V_{gc} R_L \tag{4-2}$$

and the voltage gain of the preamplifier is:

$$A_v = \frac{V_o}{V_{gc}} = \beta g_m R_L \tag{4-3}$$

From Table 3.1 it is seen that a typical value for g_m is 75 micromhos, R_L is 6.8 Kilohms and a typical Beta for the 2N1613 at these current levels is 25. Substituting these values in Eq. 4-3 yields

$$A_v = 25 \times 75 \times 10^{-6} \times 6.8 \times 10^{3} = 12.75$$

This is close to the measured voltage gain shown in Fig. 4.2, which indicates a gain of 10.

The operating voltage for the field-effect transistor was chosen as V_{ac} = 3 volts when a broadband noise measurement indicated this to be the least noisy operating point.

The circuit acts as an impedance converter, for at low frequencies the input impedance is greater than 100 megohms and the output impedance is approximately 7 kilohms. At this relatively low output impedance it is easy to take voltage readings without having pickup problems, so no further circuit complexity was introduced. This four component circuit was then completely

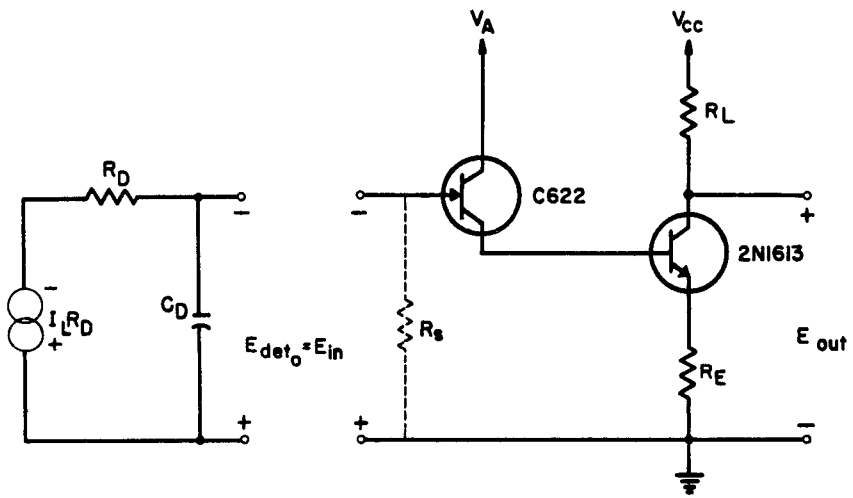

FIG. 4.1 PREAMPLIFIER SCHEMATIC

V_A = + 3 vdc
V_{cc} = + 15 vdc
R_L = 6.8 kilohms
R_E = 200 ohms
R_s = 1, 5, or 10 megohms

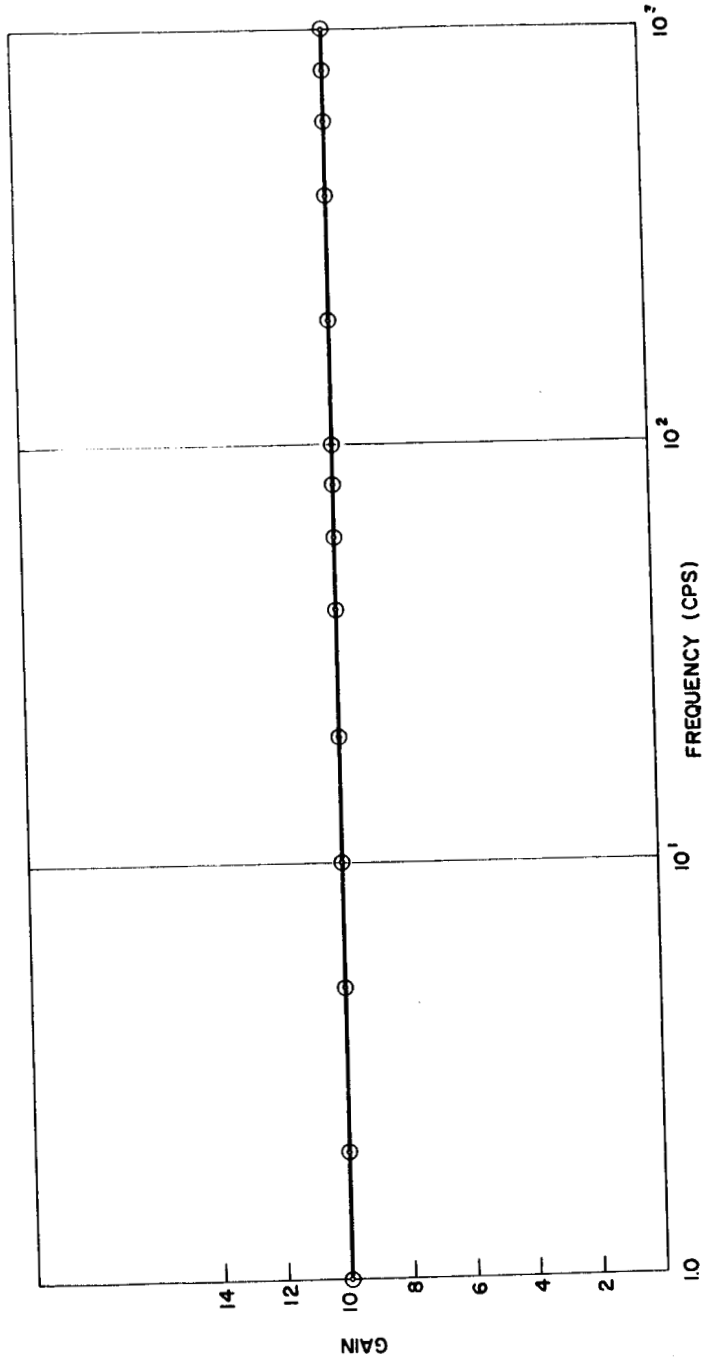

FIG. 4.2 VOLTAGE GAIN VS. FREQUENCY OF THE PREAMPLIFIER

evaluated, the results appearing in the following sections.

The shunt resistor, R_s, was used in order to make some qualitative measurements with the detector circuit and served to illustrate that the field-effect transistors, inherent high input impedance increases the sensitivity of the GaAs cell, especially at low frequency operation.

The equivalent input noise (see Appendix C) of the pre-amplifier is shown in Fig. 4.3 and the equivalent input noise power spectrum is shown in Fig. 4.4. The 1/f noise component is evident from both curves, and the amplifier is Johnson noise limited at about 1000 cycles per second.

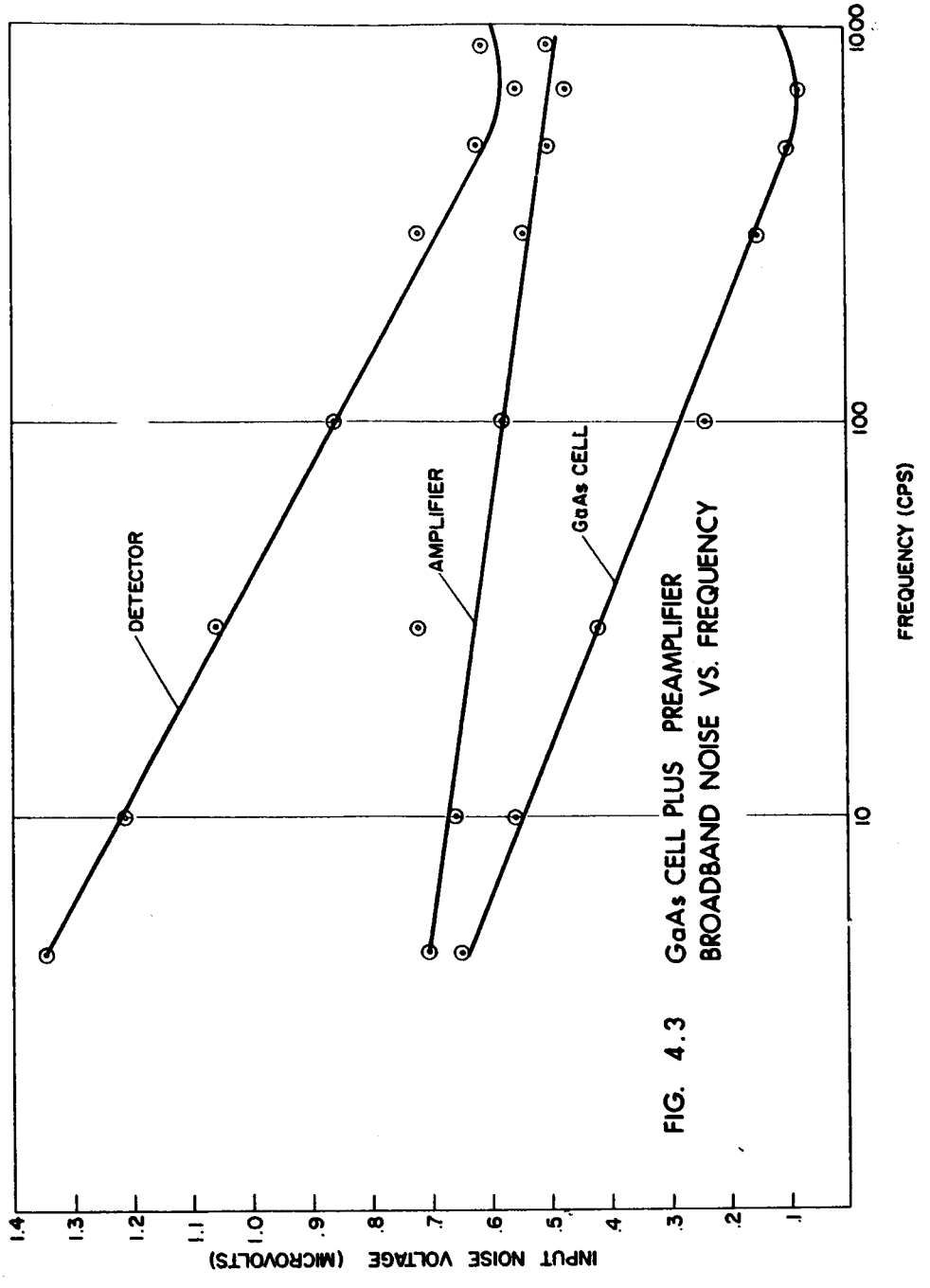

FIG. 4.3 GaAs CELL PLUS PREAMPLIFIER BROADBAND NOISE VS. FREQUENCY

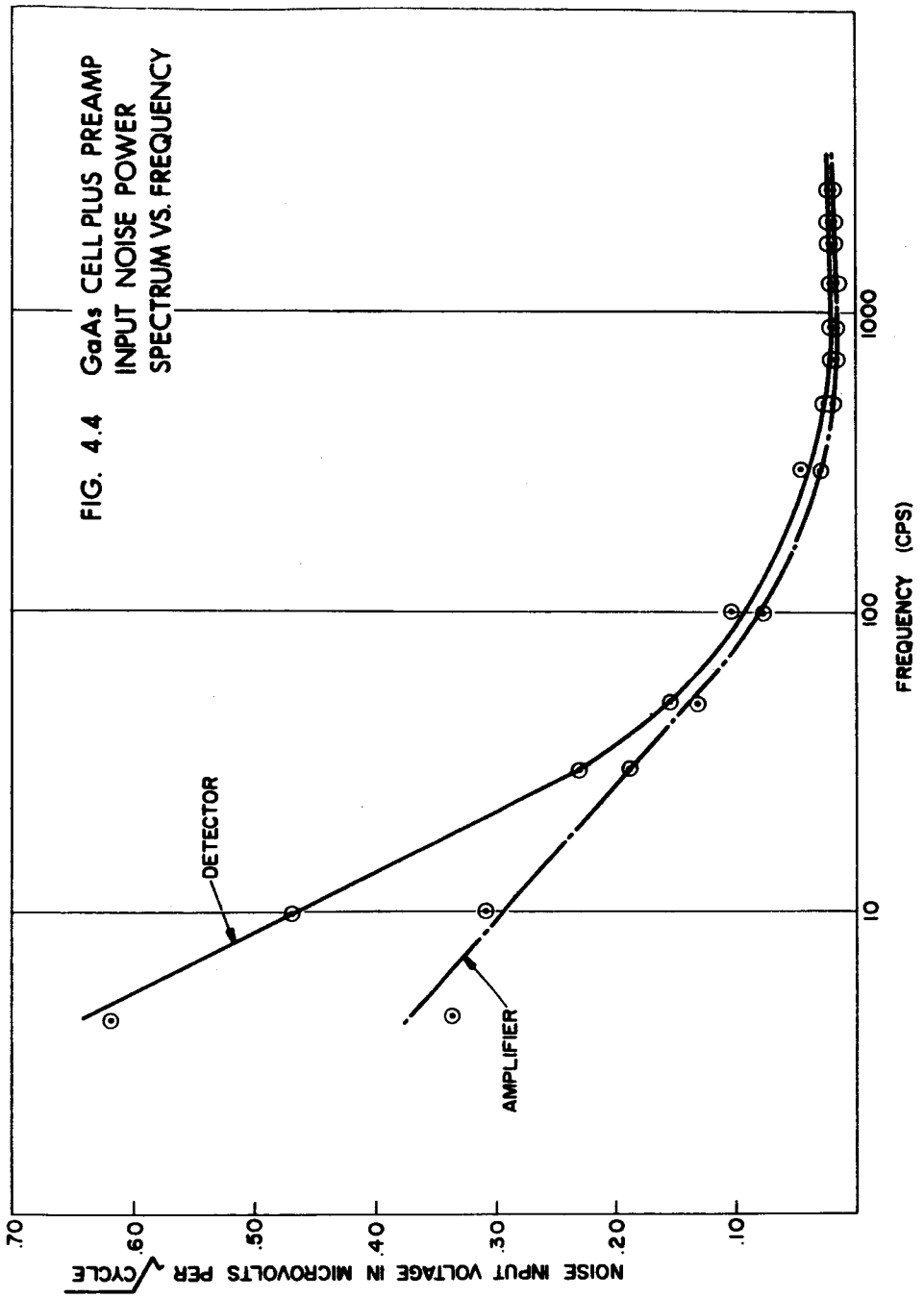
FIG. 4.4 GaAs CELL PLUS PREAMP
INPUT NOISE POWER
SPECTRUM VS. FREQUENCY
NOISE INPUT VOLTAGE IN MICROVOLTS PER √CYCLE
.70
.60
.50
.40
.30
.20
.10
10
100
1000
FREQUENCY (CPS)
DETECTOR
AMPLIFIER

4.2 The Detector

4.2.1 Noise Characteristics

The GaAs cell was connected to the preamplifier as shown in Fig. 4.1 and the combinations noise spectrum and equivalent input noise were measured. The results are shown in Figs. 4.3 and 4.4. Fig. 4.5 shows the GaAs cell's noise power spectrum and was obtained by subtracting the two curves of Fig. 4.4. The combination exhibits "1/f" noise up to about 600 cps and then becomes Johnson noise limited. The equivalent input noise for the detector at 5 cps was 1.33 microvolts while the noise at the optimum chopping frequency, that is at about 600 cps, was 0.58 microvolts. It is seen from this that the range of equivalent input noise varies by only 43% from peak (5 cps) to valley (600 cps).

4.2.2 Frequency Characteristics

The detector was placed in an enclosed housing and a fast responding (turn on time = turn off time = 100 microseconds) lamp was radiated onto the surface of the cell. (see Appendix D)

The lamp intensity was kept constant during the measurement and the shunt resistance was changed between one, five, and ten megohms, and out of the circuit entirely.

The results of this measurement are shown normalized in Figs. 4.6a and 4.6b where Fig. 4.6b indicates the low frequency response of the detector. It is evident from these figures that the F.E.T. preamplifier increases the sensitivity of the detector remarkably at low frequency, but does not offer anything over a 1, 5, or 10 megohm input impedance amplifier above a chopping frequency of 400 cps.

The rapid decrease in signal with frequency is evident from the equivalent circuit of the GaAs cell (shown driving R_s in Fig. 4.1). It is simply an RC integrator with R_s acting as a

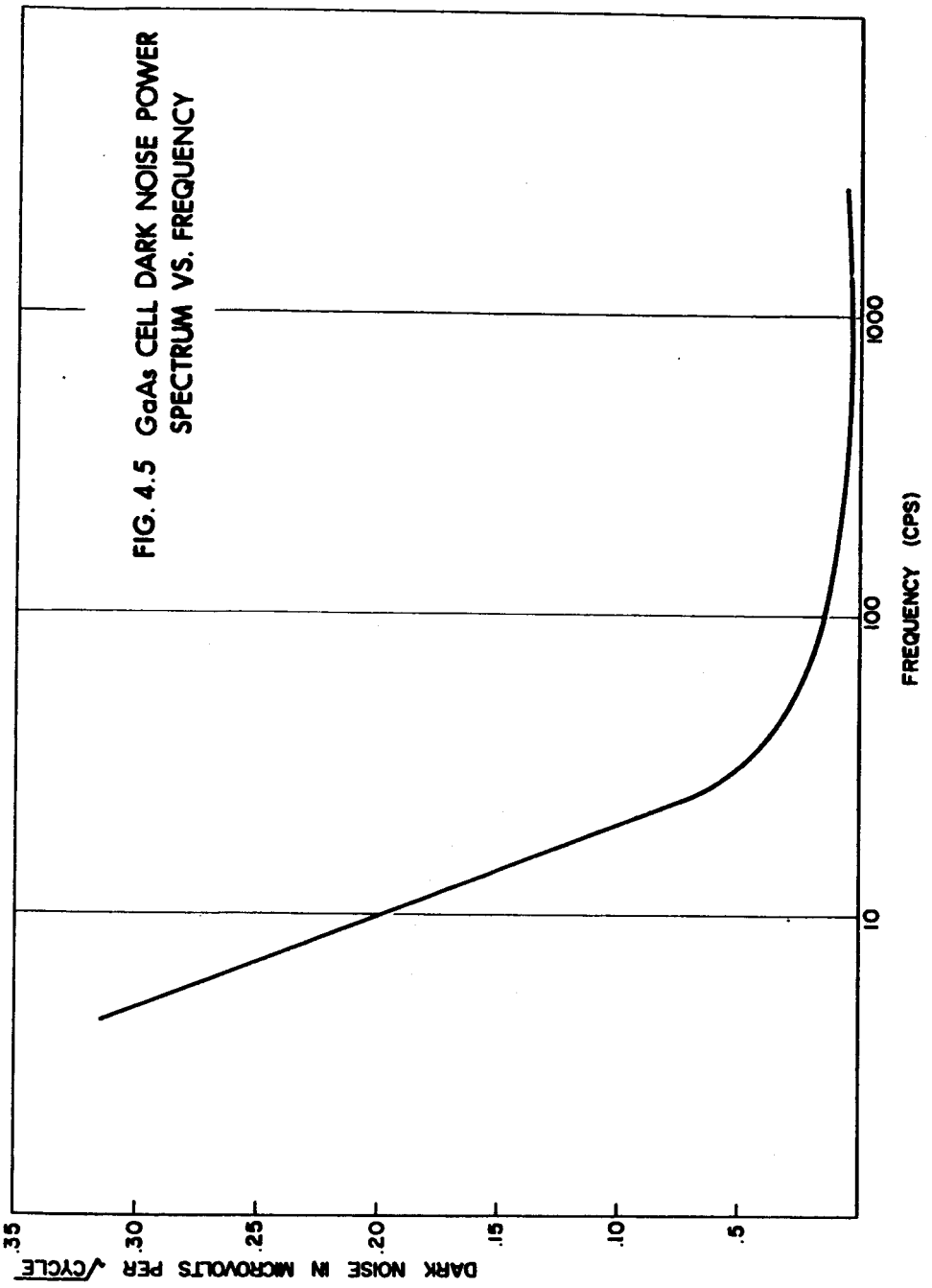
FIG. 4.5 GaAs CELL DARK NOISE POWER SPECTRUM VS. FREQUENCY
DARK NOISE IN MICROVOLTS PER √CYCLE
.35
.30
.25
.20
.15
.10
.5
10
100
1000
FREQUENCY (CPS)

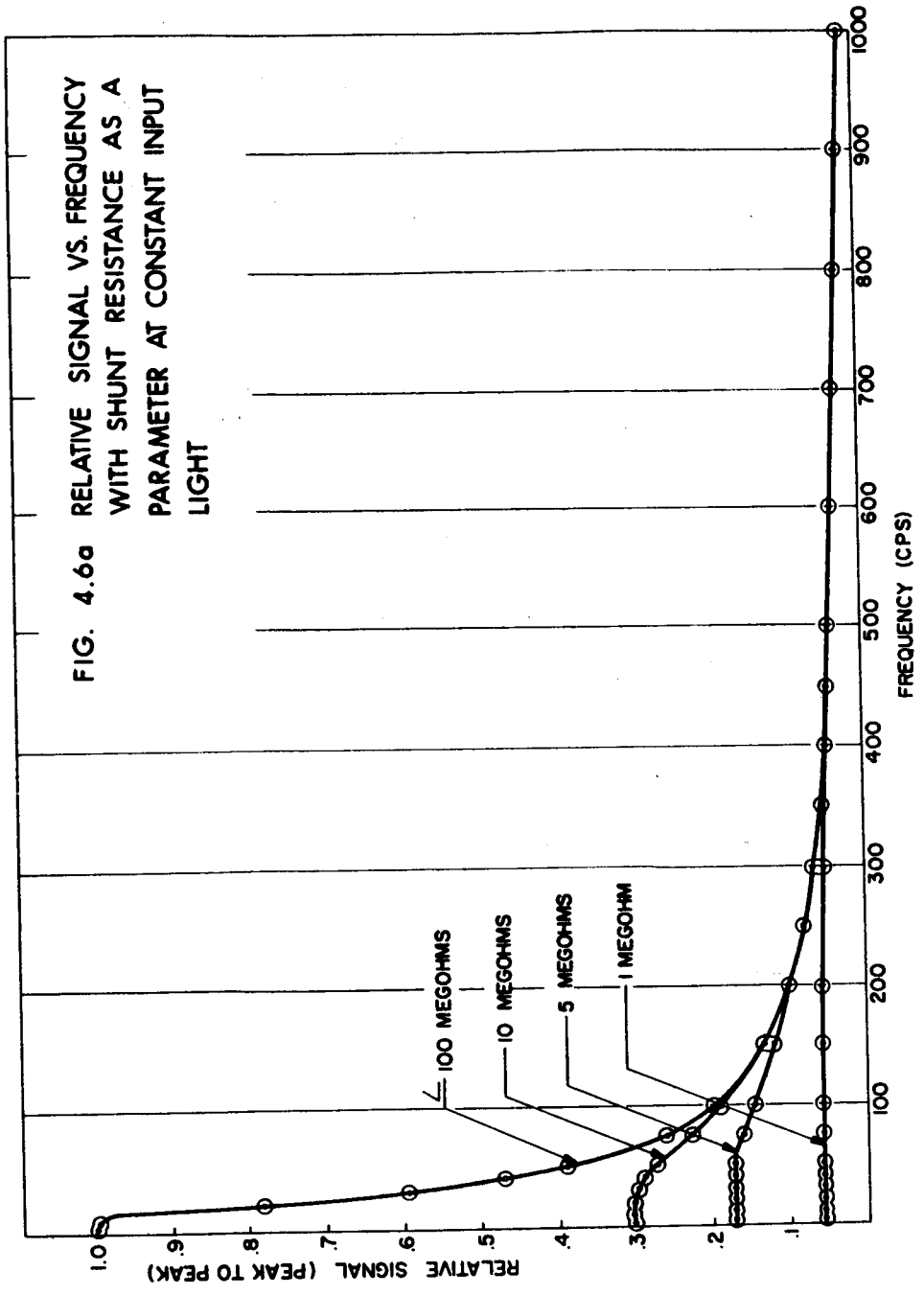
FIG. 4.6a RELATIVE SIGNAL VS. FREQUENCY WITH SHUNT RESISTANCE AS A PARAMETER AT CONSTANT INPUT LIGHT
RELATIVE SIGNAL (PEAK TO PEAK)
1.0
.9
.8
.7
.6
.5
.4
.3
.2
.1
100 MEGOHMS
10 MEGOHMS
5 MEGOHMS
1 MEGOHM
100
200
300
400
500
600
700
800
900
1000
FREQUENCY (CPS)

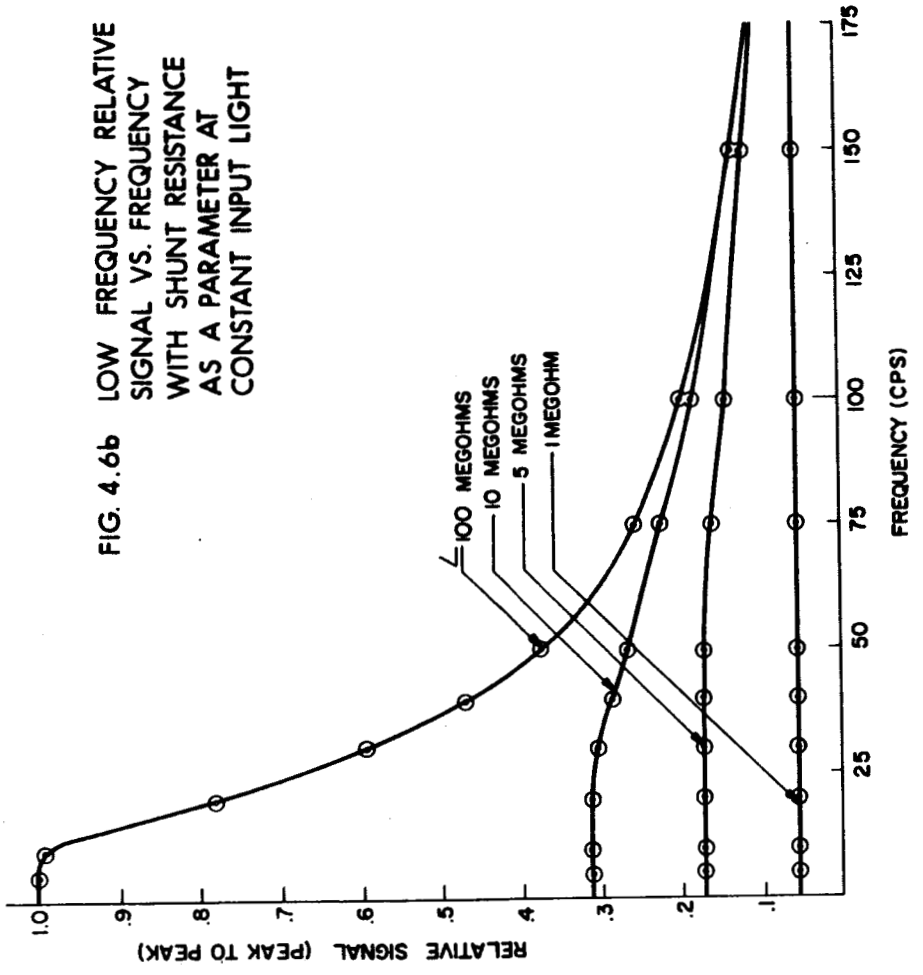
FIG. 4.6b LOW FREQUENCY RELATIVE SIGNAL VS. FREQUENCY WITH SHUNT RESISTANCE AS A PARAMETER AT CONSTANT INPUT LIGHT
100 MEGOHMS
10 MEGOHMS
5 MEGOHMS
1 MEGOHM
RELATIVE SIGNAL (PEAK TO PEAK)
1.0
.9
.8
.7
.6
.5
.4
.3
.2
.1
25
50
75
100
125
150
175
FREQUENCY (CPS)

shunt impedance across the cells output capacity. For low frequencies, Z_c, the capacitive impedance, is very high, and the output is a function of the voltage divider, namely $R_s/(R_s + R_D)$. For higher frequencies the capacitive impedance plays a more dominant role and the voltage divider is $Z_c/(Z_c + R_D)$ and independent of R_s. When $f = \frac{1}{2\pi R_s C_D}$ the signal is 3 db down.

It is clear then that only for low frequencies and direct current is the full sensitivity of the detector realizable. The detector works well at direct current; however, the problems involved with temperature stabilizing the impedance converter necessitate a much more complicated circuit. It is interesting to point out that the basic preamplifier does have some temperature gain stabilization. This comes about because the negative temperature coefficient of the tranconductance (of the field-effect transistor) is partially cancelled by the positive temperature coefficient of Beta in the 2N1613 transistor.

4. 3 Signal to Noise Ratio

The signal-to-noise ratio of the detector as a function of chopping frequency and shunt resistance is shown in Figs. 4. 7a and 4. 7b. Figure 4. 7b shows the low frequency characteristic in more detail.

The curves were generated by dividing the relative signal of Fig. 4. 6a by the equivalent input noise as found in Fig. 4. 3 and normalizing the result.

The characteristics show that the frequency at which the S/N ratio peaks is nowhere near the frequency at which the equivalent input noise bottoms. This can certainly be appreciated from the fact that the relative signal at 5 cps is unity while at 600 cps it is down to 5% of this value. For the same frequency range, it will be recalled the noise was down by 43%. It is obvious then that the peak S/N ratio will be somewhere between these two values. The full potential of this detector would be realized if the S/N ratio curve did peak at the low equivalent input noise frequency, but this can only be realized when the output capacitance of the GaAs cell can be compensated.

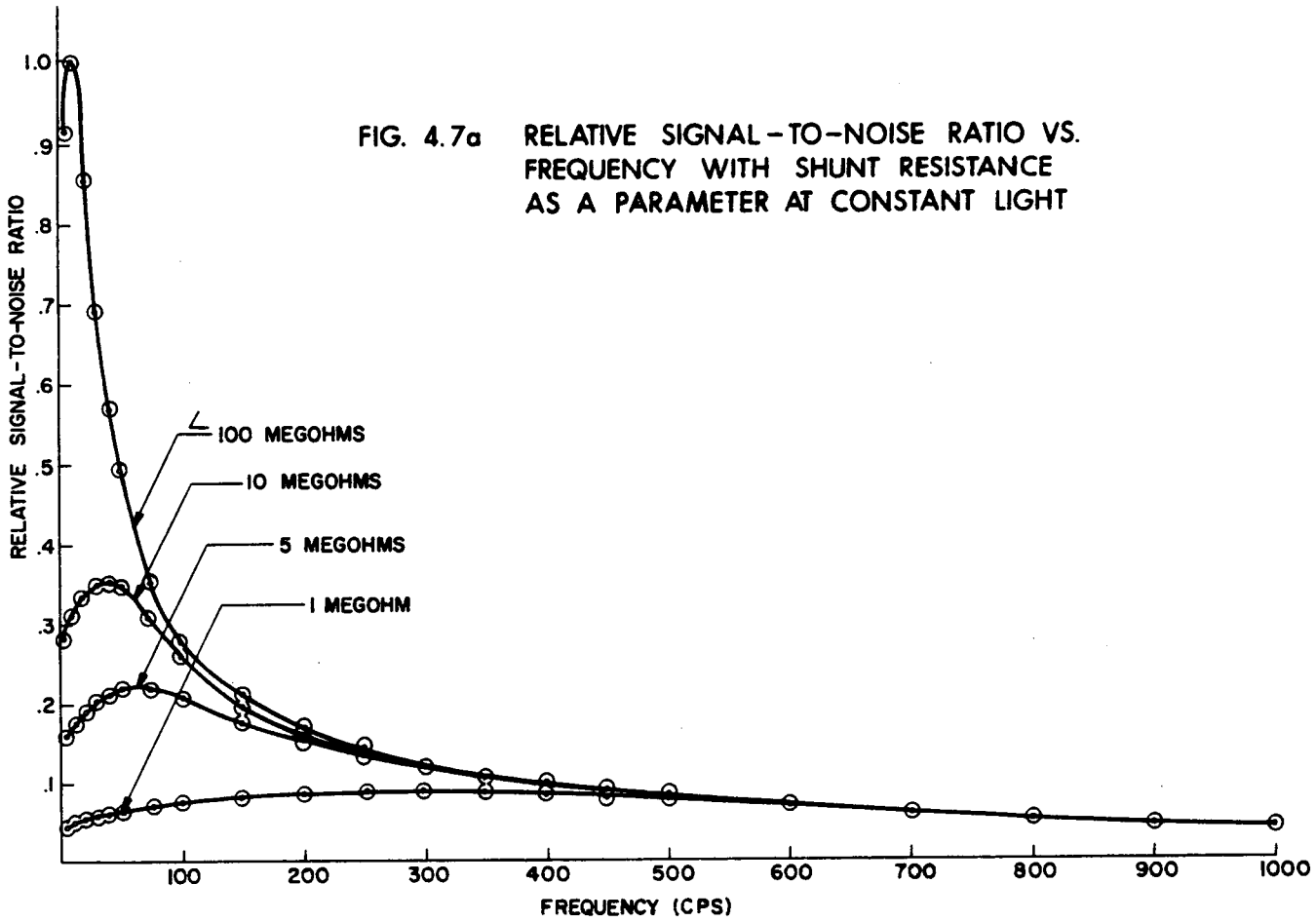

FIG. 4.7a RELATIVE SIGNAL-TO-NOISE RATIO VS. FREQUENCY WITH SHUNT RESISTANCE AS A PARAMETER AT CONSTANT LIGHT

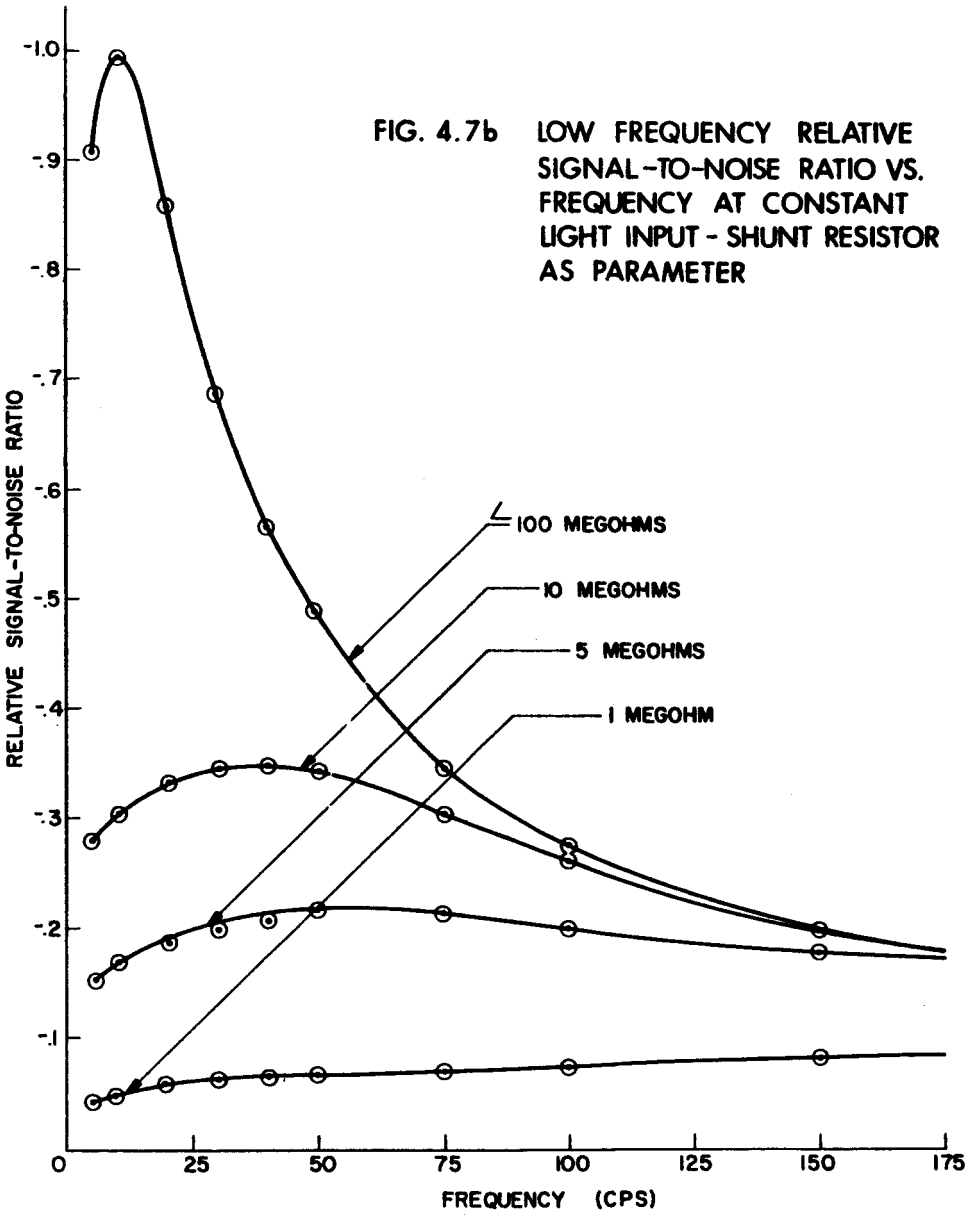

FIG. 4.7b LOW FREQUENCY RELATIVE SIGNAL-TO-NOISE RATIO VS. FREQUENCY AT CONSTANT LIGHT INPUT - SHUNT RESISTOR AS PARAMETER

CHAPTER V
SENSITIVITY OF DETECTOR

The preceding chapters have outlined the characteristics of the detector, but whether it can sense low light levels has yet to be determined.

An arbitrary but nonetheless useful comparison was made between the detector and a 1P21 photomultiplier. Because the two devices have greatly different spectral characteristics, a luminous sensitivity comparison was ruled out in favor of a radiant sensitivity comparison. The wavelength of comparison was chosen from the crossover point of the two devices' spectral characteristics plotted to a normalized scale, (see Fig. 5.1). From this figure it is seen that the crossover point is at 0.56 microns, where both devices are down 37% from their peak radiant sensitivity.

The two devices were put into similar fixtures and their sensitive surfaces were placed at the focal plane of a 60 mm objective lens. Since the 1P21 has a much larger surface area than the detector it was masked down to 1 mm^2. A 2870°K source with a 0.566 micron interference filter was placed along the optical path of the telescope, and a mechanical chopper consisting of a DC motor and a symmetrical disc with two opaque surfaces was placed in the optical path. The schematic representation of this test configuration is given in Fig. 5.2.

The detector was then placed in the optical path and with the chopper set at 5 cps, and the output driving a low pass 1 KC filter, a signal of 42 millivolts (see Fig. 5.3a) was measured. Neutral density filters were then placed in front of the objective lens until the signal as read on the oscilloscope was approximately 2.5 to 3 times the noise (Fig. 5.3b). The signal was about 3.2 mv peak to peak. A 1.9 N.D. filter was used at this test point.

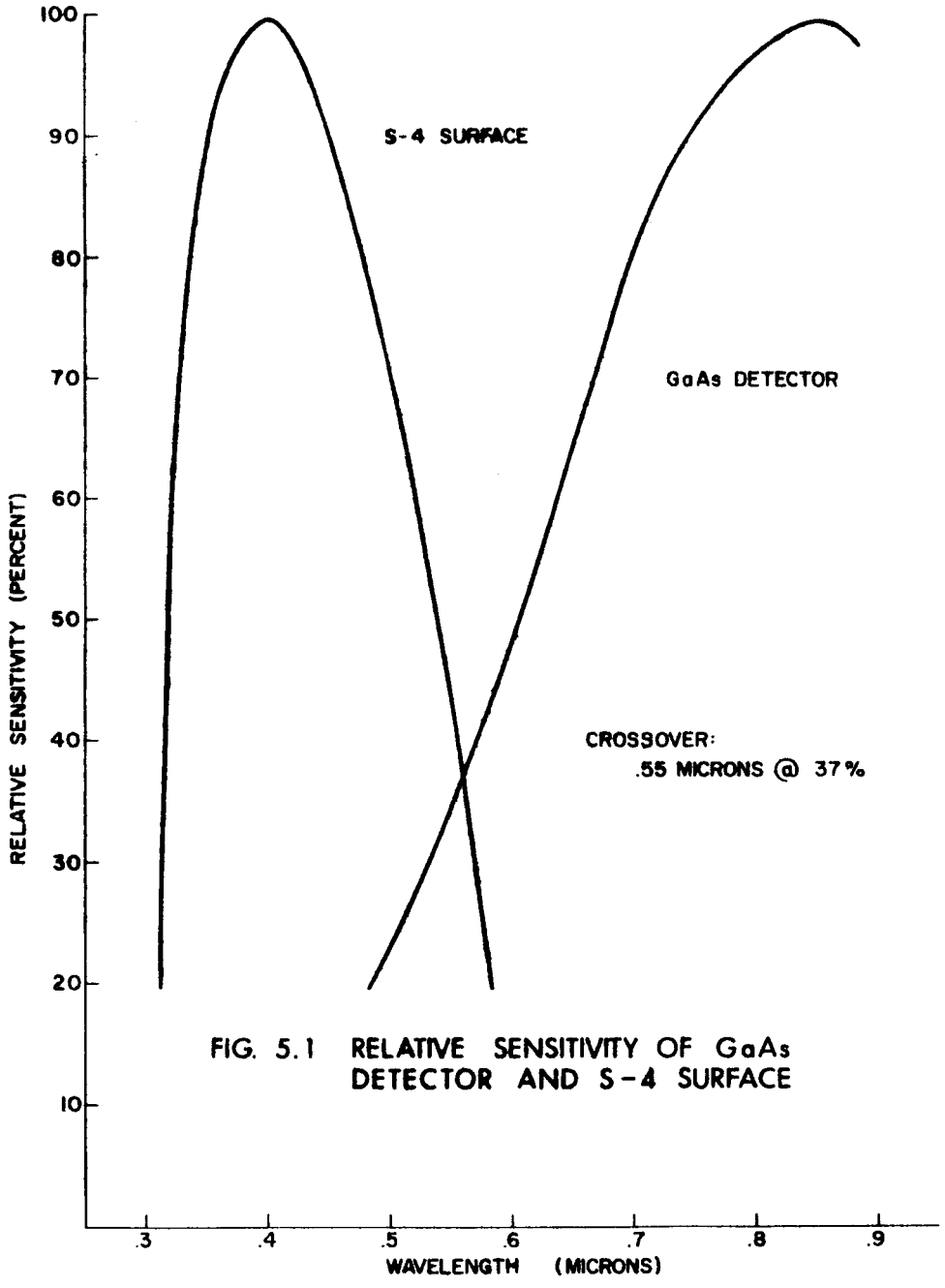

FIG. 5.1 RELATIVE SENSITIVITY OF GaAs DETECTOR AND S-4 SURFACE

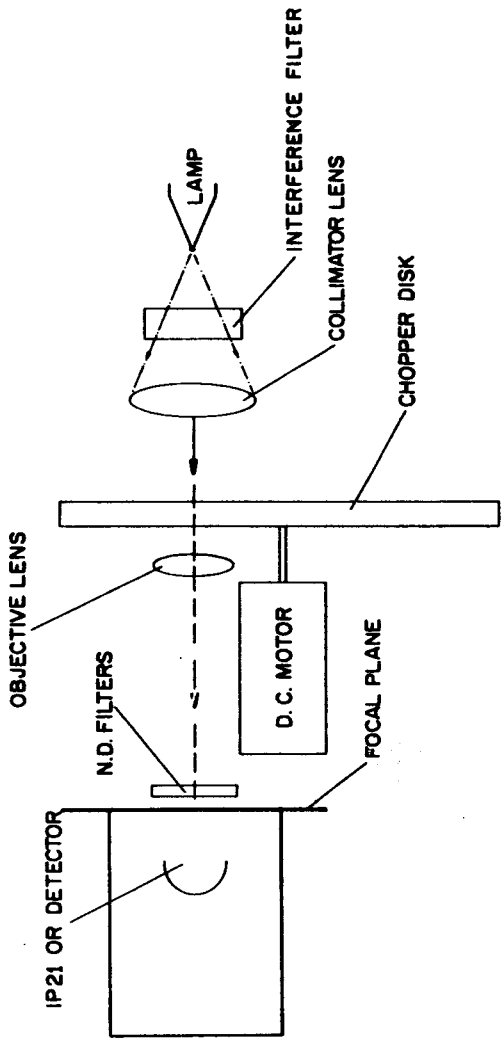

FIG. 5.2 OPTICAL CONFIGURATION FOR THE RADIANT SENSITIVITY TEST

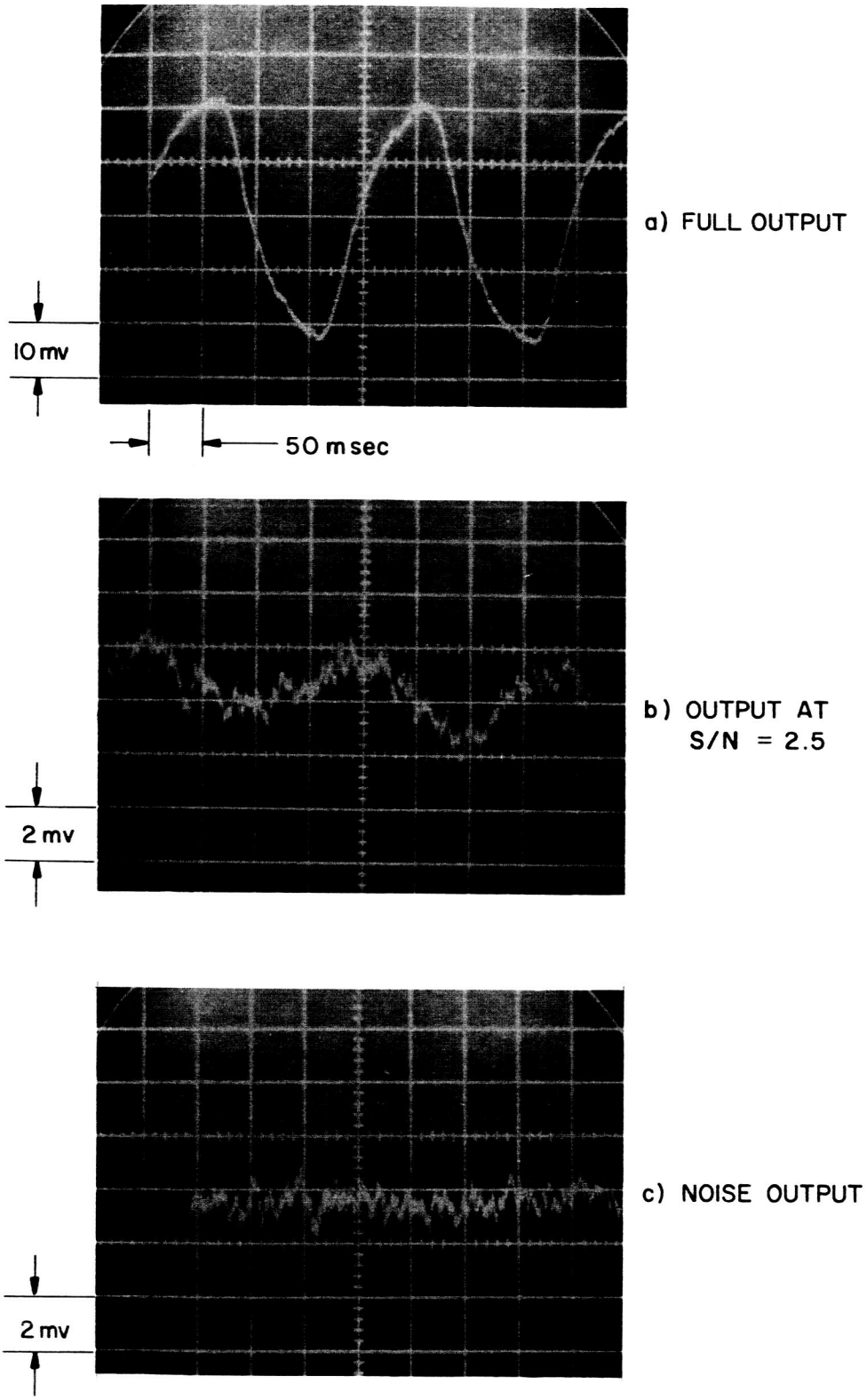

FIG. 5.3 OSCILLOSCOPE TRACES OF DETECTOR SENSITIVITY TEST

The detector was then replaced by the 1P21, and,with the same initial light level, chopping frequency and output filtering as was used on the detector,a measurement was made. The output from the 1P21 was 42 volts (see Fig. 5. 4a). It should be noted that the ratio of the two detectors output signals is a nebulous quantity since both are relatively noise free signals and easily measurable. Neutral density filters were again placed in front of the objective lens until the point was reached where the output from the filter was 2. 5 to 3 times the noise (see Fig. 5. 4b). A 3. 4 N. D. filter was needed for this test point.

A 42 volt output signal from the 1P21 corresponds to a 42 microamp anode current since the anode resistor was 1 megohm. The median radiant sensitivity of the 1P21 at 0. 4 microns is 78, 000 microamps/microwatt. However, at 0. 566 microns, the wavelength at which this measurement was made, the radiant sensitivity is down to 34% of its peak value as seen from Fig. 5. 1.

The power being sensed by the 1P21 and consequently by the detector at this test point is then given by

$$P = \frac{I}{S_K} = \frac{42 \times 10^{-6} \quad a}{0.34 \times 78 \times 10^{3} \frac{\mu a}{\mu w}} \approx 1.6 \times 10^{-9} \text{ watts} \qquad (5\text{-}1)$$

The lower limit power for the detector at the S/N = 2. 5 point is

$$P_{LLD} = \frac{1}{10^{N.D.}} P$$

or

$$P_{LLD} = \frac{1}{10^{1.9}} \times 1.6 \times 10^{-9} = 2 \times 10^{-11} \text{ watts} \qquad (5\text{-}2)$$

giving a detector sensitivity of

$$S_{DR} = \frac{2 \times 10^{-11}}{0.707 \times 3.2 \times 10^{-3}} = 0.9 \times 10^{-8} \frac{\text{watts}}{\text{rms volt}}$$

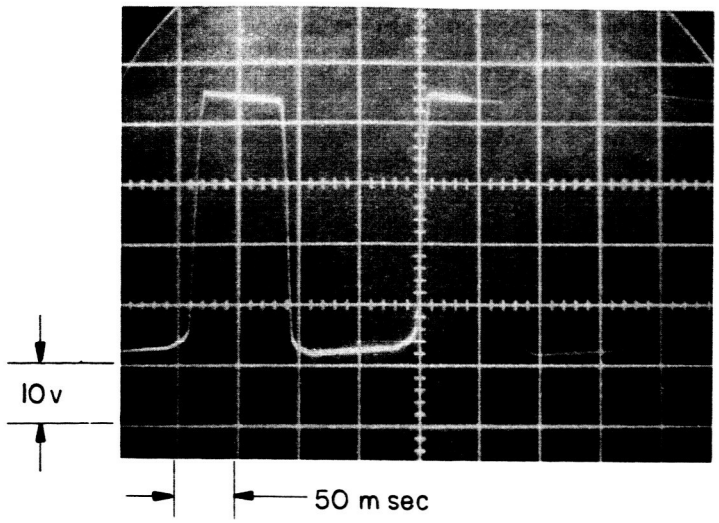

a) FULL OUTPUT

10v

50 m sec

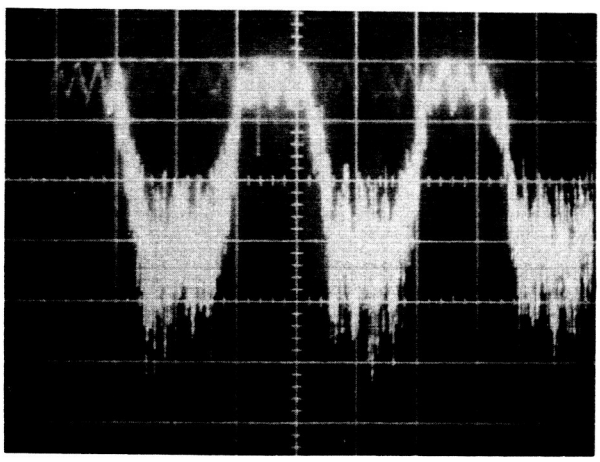

b) OUTPUT AT S/N = 2.5

20mv

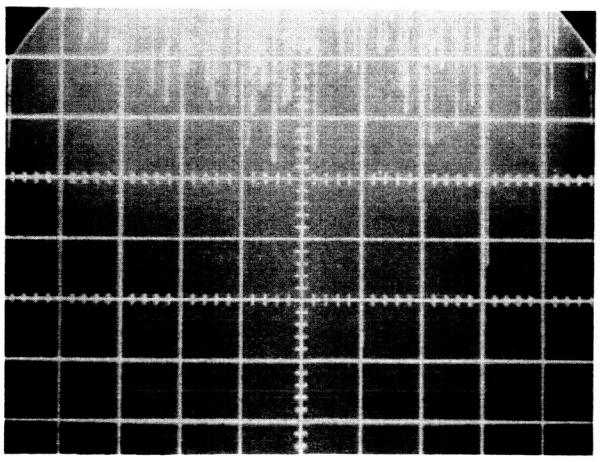

c) SHOT NOISE

20mv

FIG. 5.4 OSCILLOSCOPE TRACES OF IP21 SENSITVITY TEST

The lower limit on the power that the 1P21 sensed was

$$P_{LLM} = \frac{1}{10^{3.4}} \times 1.6 \times 10^{-9} = 0.64 \times 10^{-12} \text{ watts}$$

This comparison clearly indicates that the 1P21 is more sensitive than the detector at this wavelength. However, these power limits should not be construed as the ultimate lower level capable of being sensed, for just as the photomultiplier tube can sense lower levels by using a narrower bandwidth, so can the detector.

The results of the measurements are given in Figs. 5.5 and 5.6. These curves are the same as Figs. 4.6a and 4.7b, but with the ordinate dimensions being minimum power and S/N ratio respectively, at the measurement test point.

The S/N ratio decreases with higher chopping frequencies and/or lower input impedance amplifiers at 2×10^{-11} watts incident to the surface, (see Fig. 5.5); whereas the lowest detectable power at a constant S/N ratio increases. The luminous sensitivity of the detector at 0.566 microns is, using the conversion 1 watt = 621 lumens:

$$S_{DL} = 621 \times S_{DR}$$

$$S_{DL} = 621 \times 0.9 \times 10^{-8} = 5.6 \times 10^{-6} \frac{\text{lumens}}{\text{rms volt}} \qquad (5\text{-}3)$$

The rms output signal was 0.707×3.2 mv = 2.25 mv. The luminous equivalent at the S/N = 2.5 point is then $2.25 \times 10^{-3} \times 5.6\ 10^{-6}$ $= 1.36 \times 10^{-8}$ lumens. Equating this to Fabre's number, with 100mm optics, will give the magnitude of star that can be sensed with the detector at a 5 cps chopping speed and Δf = 1000 cps:

$$F A_{o1} = L_p$$

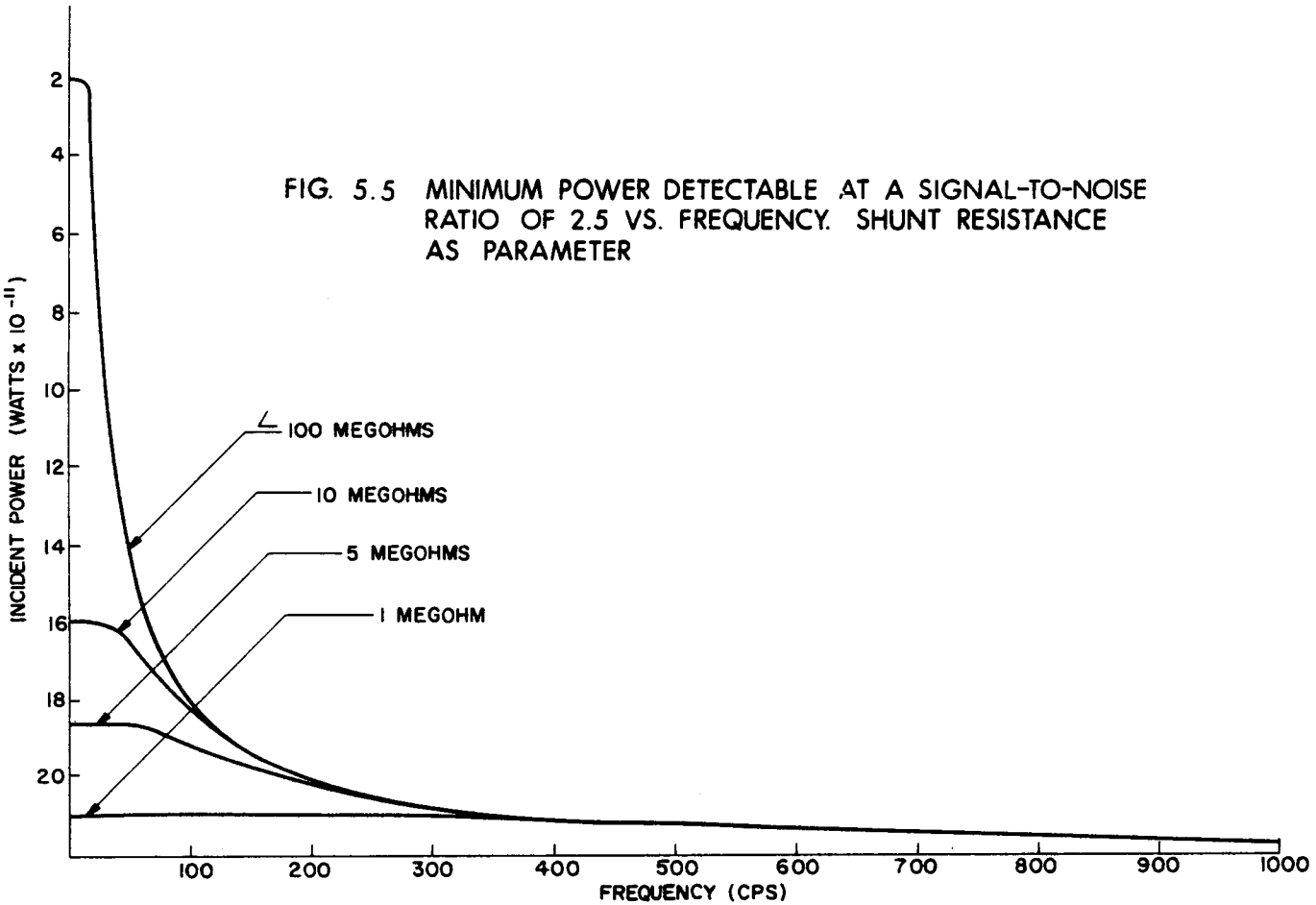

FIG. 5.5 MINIMUM POWER DETECTABLE AT A SIGNAL-TO-NOISE RATIO OF 2.5 VS. FREQUENCY. SHUNT RESISTANCE AS PARAMETER

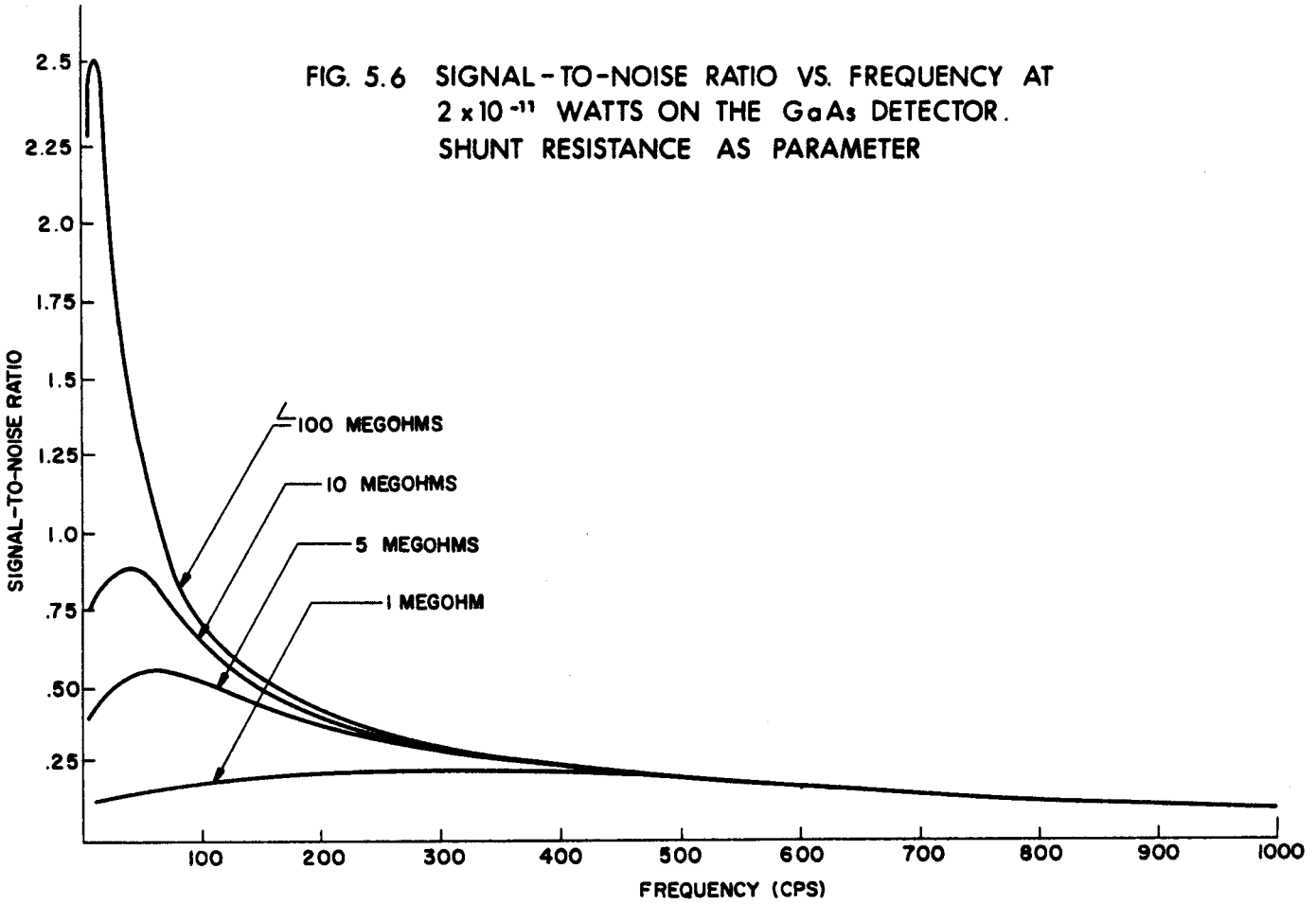

FIG. 5.6 SIGNAL-TO-NOISE RATIO VS. FREQUENCY AT 2×10^{-11} WATTS ON THE GaAs DETECTOR. SHUNT RESISTANCE AS PARAMETER

or

$$\frac{8.3 \times 10^{-7}}{2.5^{m_v - 1}} \times \frac{\pi}{4}(10^{-1})^2 = 1.36 \times 10^{-8} \qquad (5\text{-}4)$$

and $m_v \doteq 0.2$

If the bandwidth is limited to 1 cps and the signal to noise ratio kept the same, the signal voltage would be

$$e_s = \frac{S}{N} \; e_{nrms} \; A_v \qquad (5\text{-}5)$$

where e_{nrms} from Fig. 4.3 is 1.33μv, and A_v is the gain of the preamplifier and equal to 10. The luminous flux is then

$$L_p = S_{DL} \; e_s = S_{DL} \; \frac{S}{N} \; e_{nrms} \; A_v$$

Then the magnitude of star that can be sensed is given by

$$\frac{8.3 \times 10^{-7}}{2.5^{m_v - 1}} \times \frac{\pi}{4}(10^{-1})^2 = (5.6 \times 10^{-6})(2.5)(1.3 \times 10^{-6})(10)$$

and $m_v = 4.9$ is the theoretical lower limit of stellar magnitude at 5 cps chopping frequency and a bandwidth of 1 cps.

CHAPTER VI
CONCLUSIONS AND RECOMMENDATIONS

By using a very high input impedance field effect transistor amplifier in conjunction with a gallium arsenide photovoltaic cell, a low level light sensor was built that could sense stellar radiation.

In order to fully utilize the sensitivity of the detector, its output capacitance must be compensated. This would give a flat signal vs frequency characteristic (see Fig. 4.6a) and would allow the detector to be chopped at the optimum low noise frequency. This would make the sensing (at f = 600 cps, Δf = 1 cps, O.L. = 100 mm) of a 5.8 magnitude star theoretically possible.

The cell's output capacitance could be compensated for by using a negative capacitance amplifier or by tuning the capacitor to the chopping frequency with an inductive shunt.

These solutions will, however, add a great deal of complexity to the preamplifier, and by far the best solution would be to lower the inherent junction capacity of the cell. With the advent of epitaxial and planar techniques in the transistor industry, this should be forthcoming.

It is also recommended that fuller advantage be taken of the negative temperature coefficient of the transconductance of the field-effect transistor when it is coupled to a conventional transistor. If the two devices were diffused into the same silicon chip, complete temperature compensation could be achieved giving a rather universally useful temperature compensated DC and AC amplifier.

Finally, work can be done in determining whether the use of devices whose spectral characteristics go into the infrared can be more fully utilized as star sensors. This would entail the compilation of data on many stars of visible magnitude, determining how far out their spectrum goes and whether by using their

infrared content their S/N ratio is enchanced.

APPENDIX A
FIGURES OF MERIT[3, 8]

Because the requirements are so diverse, several figures of performance have been developed for use in comparing one detector with others of the same or similar type. The following definitions and functional relationships are given for those which are considered to be the most pertinent in modern day use.

1. Responsivity

The responsivity is defined as*

$$R = \frac{V}{JA} \quad \frac{\text{Volts}}{\text{Watts}} \tag{A-1}$$

Responsivity, the ratio of the rms value of the fundamental component of the signal voltage to the rms value of the fundamental component of the incident radiation power, is written in functional notation as

$$R = R(b, \lambda, f)$$

2. Noise Equivalent Irradiance

The noise equivalent irradiance is defined as

$$NEI = H_N = \frac{NJ}{V(\Delta f)^{1/2}} \quad \frac{\text{Watts}}{\text{cps}^{1/2}\,\text{cm}^2} \tag{A-2}$$

H_N is the minimum radiant flux density necessary to produce a signal-to-noise ratio of 1 when the noise value is normalized to a unit bandwidth. In functional notation

$$H_N = H_N(b, \lambda, f, A)$$

Since the area of the detector is not taken into account in H_N, the figure describes the performance of a detector of a specific

*A list of symbols for Appendices A and B appears at the end of Appendix A.

area.

3. Noise Equivalent Power

The noise equivalent power is defined as

$$NEP = P_N = \frac{NJA}{V(\Delta f)^{1/2}} \quad \frac{Watts}{(cps)^{1/2}} \qquad (A-3)$$

P_N is the minimum radiant flux necessary to produce a signal-to-noise ratio of 1 when the noise value is normalized to unit bandwidth. In functional notation

$$P_N = P_N(b, \lambda, f)$$

4. D-Star

D-Star, or D*, is defined as

$$D^* = \frac{A^{1/2}}{NEP} = \frac{cm\ cps^{1/2}}{Watts} \qquad (A-4)$$

D* is the detectivity normalized to unit area and unit bandwidth. Detectivity is the signal-to-noise ratio produced with unit radiant flux incident on the detector. Since the area dependence of the signal-to-noise ratio has been taken into account, D* describes the general detector type rather than a detector of some particular area.

In functional notation

$$D^* = D^*(b, \lambda, f)$$

Symbol Definitions for Appendices A and B

A	area of the detector in cm^2
b	bias applied to the detector
f	modulation frequency of the radiation incident on the detector
Δf	frequency bandwidth of the electrical measuring system in cps

J	radiation flux density in watts/cm^2
N	noise of the detector in volts
V	signal of the detector in volts
λ	wavelength, in vacuum, of the radiation incident on the detector.

APPENDIX B

DEFINITION AND TYPE OF NOISE FOUND IN DETECTORS[3, 8, 15]

Fluctuations in the observable parameters or "noise" are what essentially limit the detectivity of detectors. While the several performance figures perform an important and valuable function for comparison and tabulation of large varieties and quantities, the noise power spectrum should be considered no less important. The following noises are commonly found in detectors or more generally in electronics:

$$1.\quad \overline{N^2}_{f^{-1}} = \alpha_1 (i^x / f^g)\Delta f \qquad \text{(B-1)}$$

where x = 2 generally and y = 1 although variations from these values have been noted. This noise is commonly called "one over f" (1/f) noise and is generally attributed to surface effects and faulty contacts.[4]

$$2.\quad \overline{N^2}_{N-J} = 4kTR\Delta f \qquad \text{(B-2)}$$

where k is the Boltzmann constant, T is absolute temperature, and R is the resistance of circuit. Electrical fluctuations in element occur at thermal equilibrium, hence known as thermal noise, better known as Nyquist-Johnson noise. This type of noise has no frequency dependence except at high frequencies when R should be replaced by the circuit impedance.

$$3.\quad \overline{N_r^2} = \alpha b^x r^2 \Delta f \qquad \text{(B-3)}$$

where b is an applied bias, α and x are constants, and r is the detector response. This general type of noise could well be known as signal noise but is sometimes called response noise because it is caused by fluctuations in the incident radiation or in the fundamental mechanism of the detector and will, therefore, be porportional to responsivity and have the same frequency

characteristic.

Detectors in the range where they are response noise limited will have a flat detectivity frequency spectrum.

The general class of response noise includes the following:

1. Noise due to Brownian motion of a diaphragm or similar element.

2. Noise due to fluctuation in power flowing to and from the sensitive element.

3. Generation-recombination noise (G-R) which includes fluctuation in carrier concentrations caused by emission and absorption of lattice phonons and by absorption of background radiation photons. (If the latter noise is limiting, the detector is said to be background limited.)

4. Noise due to fluctuations in the incident radiation signal (the ultimate limiting noise sometimes called photon noise).

Response noise indicates the fundamental limitation on detectivity for the particular detector considered. When this condition prevails, such action as cooling the lattice, restricting the field of view, or modifying the thermal conductance path,etc., can result in performance improvement.

APPENDIX C
NOISE MEASUREMENT TECHNIQUE

The schematic diagram of the noise measurement test circuit is shown in Fig. C. 1. The output of the detector was fed into a Philbrick pass band (Δf = 3000 cps) constant gain (Av = 150) amplifier. The output from the amplifier went to a high Q variable filter and the output from this was DC restored. The result was fed into a thirty three second integrator and displayed on an oscilloscope. For all frequency settings the input to the integrator was $e_{np}(-1 + \sin 2\pi ft)$ where e_{np} was the peak noise voltage.

By choosing the integration time to be very much larger than the period of the lowest frequency to be measured, the circuit was able to smooth the random noise voltage output and make it a rather straightforward measurement technique.

The equation of the signal that was displayed on the oscilloscope was

$$e = K_1 \int_0^{t_1} e_{np}(-1 + \sin 2\pi ft)\, dt$$

$$= K_1 \left[e_{np} t_1 - \frac{e_p}{2\pi f} \cos 2\pi ft \right] \qquad \text{(C-1)}$$

This signal is seen to be composed of a ramp that has superimposed upon it an AC signal at the noise frequency being measured. The time of integration, t, was 28 seconds and the constant, K_1, was composed of the gain of the measurement circuit.

To get a measurement test point then, the high-Q filter was set at a frequency, and the integrator was discharged, after which the output started to rise. When the constant slope signal crossed the 28 second time mark a voltage reading was taken. This reading was related to the noise signal by

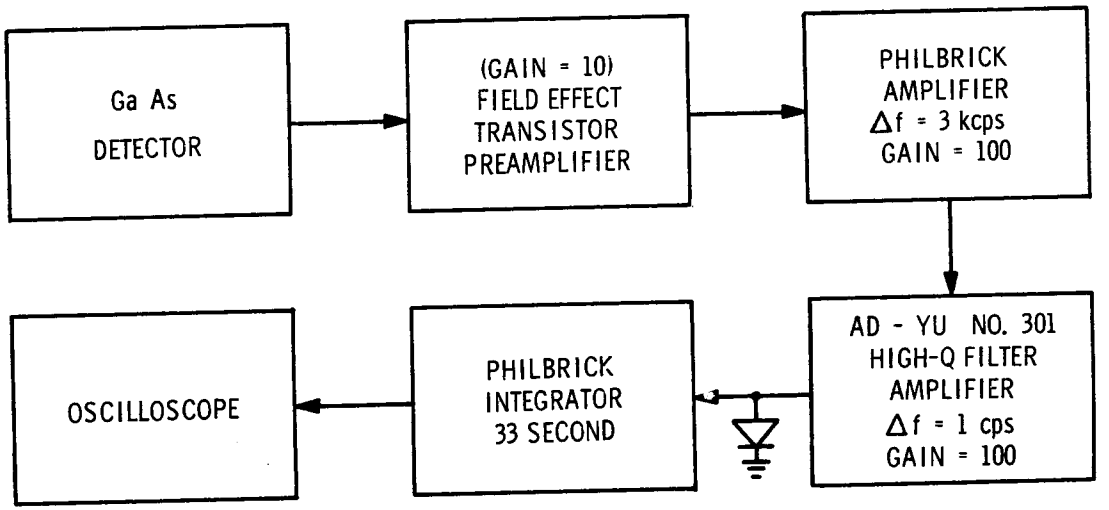

FIG. C.1 NOISE MEASUREMENT TEST CIRCUIT

$$e = K_1 e_{np} t_1 \qquad K_1 = 1.5 \times 10^4 \text{ , } t_1 \text{, } = 28 \text{ seconds}$$

Therefore

$$e_{np} = \frac{e}{K_1 t_1}$$

and

$$e_{nrms} = .707\, e_{np} = .707\, \frac{e}{K_1 t_1}$$

This technique was followed over the frequency range and resulted in Figs. 4.3, 4.4, and 4.5.

APPENDIX D
FREQUENCY RESPONSE TEST CIRCUIT

As outlined in Fig. D. 1, the circuit used consisted of a sinusoidal oscillator driving a Schmitt trigger whose output went to the grid of an Amperex type 6977 indicator tube. This tube is similar to a vacuum tube triode and when a positive signal is applied to the grid, the tube bottoms and a current of about 600 μa is drawn to the anode. The anode is coated with a P15 phosphor and glows at a peak wavelength of 0. 5 microns when this current flows. The typical light output of the tube is 3 ft-lamberts. The tube turns on and off (when a negative signal is applied to the grid) in approximately 100 microseconds.

The indicator tube and the detector were placed in a light-tight enclosure. The frequency to the grid was then varied and the detector output recorded. The intensity was monitored by a photomultiplier and was constant over the frequency range used in the measurement. The results of this frequency response measurement are seen as Figs. 4. 6a and 4. 6b.

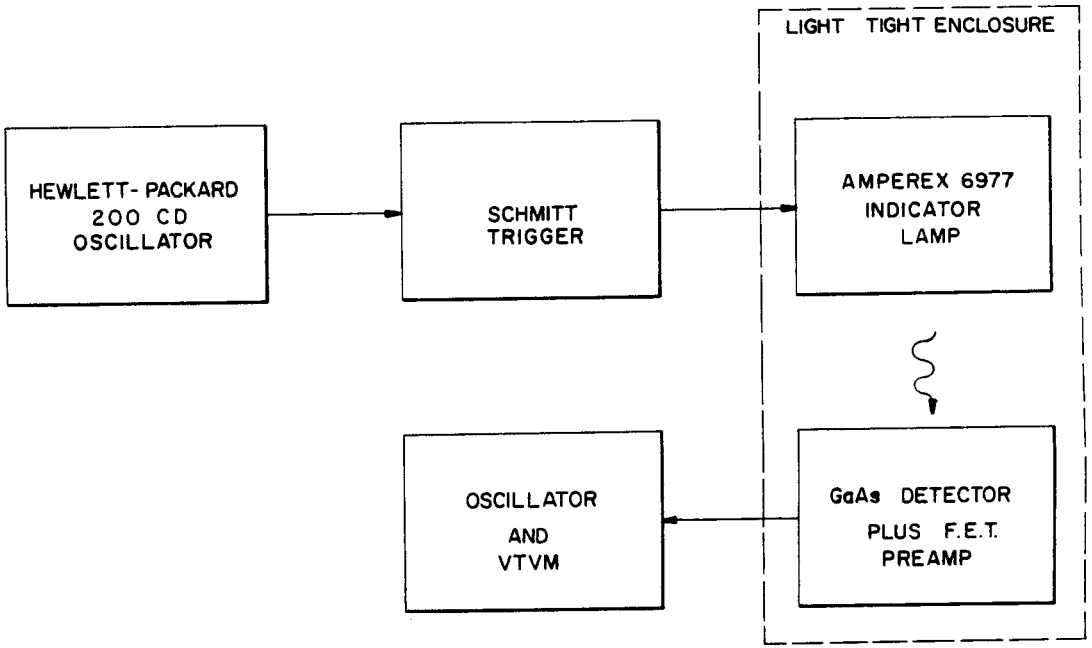

FIG. D.1 FREQUENCY RESPONSE TEST CIRCUIT

BIBLIOGRAPHY

1. Hardy and Perrin, The Principles of Optics, (McGraw-Hill, New York, 1932).

2. G. R. Pruett and R. L. Petritz, "Detectivity and Preamplifier Considerations for Indium Antimonide Photovoltaic Detectors," Proceedings of IRE, Vol. 47, No. 9, 1959, pp. 1524-1529.

3. R. Potter and N. Eisenman, "Infrared Photodetectors: A Review of Operational Detectors," Applied Optics, Vol. 1, No. 5, September 1962, pp. 567-574.

4. P. Bratt, W. Engeler, H. Levinstein, A. MacRae and J. Pehek, "A Status Report of Infrared Detectors," Infrared Physics, Vol. 1, 1961, pp. 27-38.

5. Kruse, McGlouchlin, McQuistan, Elements of Infrared Technology, (John Wiley and Sons, Inc., New York, 1962, chapters 7-10).

6. William Shockley, Electrons and Holes in Semi-Conductors, (Van Nostrand, New York, 1950).

7. Millman and Taub, Electrical and Electronic Engineering Series, (McGraw-Hill, Inc., New York, 1956).

8. R. J. Cashman, "Film-Type Infrared Photo-Conductors," Proceedings of IRE, Vol. 47, No. 9, 1959, pp. 1471-1474.

   F. F. Rieke, L. H. DeVaux and A. J. Tuzzolino, "Single-Crystal Infrared Detectors Based Upon Intrinsic Absorption," Ibid, pp. 1475-1478.

   R. Clark Jones, "Phenomenological Description of the Response and Detecting Ability of Radiation Detectors," Ibid, pp. 1495-1502. "Noise in Radiation Detectors," pp. 1481-1486.

9. D. Sawyer and R. Rediker, "Narrow Band Ge Diodes," Proceedings of IRE, Vol. 46, No. 6, 1958, pp. 1122-1130.

10. G. Lucovsky and P. H. Cholet, "GaAs, A Sensitive Photo-diode for the Visible," Journal of the Optical Society of America, Vol. 50, No. 10, pp. 979-983.

11. Shockley, W., "A Unipolar Field Effect Transistor," Proceedings of IRE, Vol. 40, No. 11, 1952, pp. 1365-1376.

12. Shockley, W. and R. C. Prim, "Joining Solutions at the Pinch Off Point in Field Effect Transistors," IRE Transactions on Electron Devices, December 1953, pp. 1-14.

13. Dacey and Ross, "Unipolar Field Effect Transistors," Proceedings of IRE, Vol. 41, No. 8, 1953, pp. 970-979.

14. "Low Noise Silicon Field Effect Transistors," Crystalonics Technical Bulletin, F102-1163, Cambridge, Massachusetts.

15. Bell, T., Electrical Noise, (Van Nostrand, New York, 1960).